bioRxiv preprint doi: https://doi.org/10.1101/665976; this version posted June 10, 2019. The copyright holder for this preprint (which was not certified by peer review) is the author/funder. All rights reserved. No reuse allowed without permission.

Left prefrontal connectivity links subthalamic stimulation with depressive symptoms in Parkinson's disease

Friederike Irmen[1,2,3*], Andreas Horn[1*], Philip Mosley[4,5], Alistair Perry[6,7], Jan Niklas Petry-Schmelzer[8], Haidar S. Dafsari[8], Michael Barbe[8], Veerle Visser-Vandewalle[9], Gerd-Helge Schneider[10], Ningfei Li[1], Dorothee Kübler[1], Gregor Wenzel[1], Andrea Kühn[1,2,11]

[1] Department of Neurology, Charité – Universitätsmedizin Berlin, corporate member of Freie Universität Berlin, Humboldt-Universität zu Berlin, and Berlin Institute of Health, Germany
[2] Berlin School of Mind and Brain, Humboldt-Universität zu Berlin, Germany
[3] Department of Biological Psychology and Cognitive Neuroscience, Freie Universität Berlin, Germany
[4] Systems Neuroscience Group, QIMR Berghofer Medical Research Institute, Herston, Queensland, Australia
[5] Queensland Brain Institute, University of Queensland, St Lucia, Queensland, Australia.
[6] Max Planck UCL Centre for Computational Psychiatry and Ageing Research, Max Planck Institute for Human Development, Berlin, Germany
[7] Center for Lifespan Psychology, Max Planck Institute for Human Development, Berlin, Germany
[8] University of Cologne, Faculty of Medicine and University Hospital Cologne, Department of Neurology, Cologne, Germany
[9] Dep. of Stereotactic and Functional Neurosurgery, University Hospital Cologne, Cologne, Germany
[10] Department of Neurosurgery, Charité – Universitätsmedizin Berlin, corporate member of Freie Universität Berlin, Humboldt-Universität zu Berlin, and Berlin Institute of Health, Germany
[11] Deutsches Zentrum für Neurodegenerative Erkrankungen, Berlin, Germany

Corresponding author:

Friederike Irmen
Movement Disorder and Neuromodulation Unit
Charité, University Medicine Berlin
Department of Neurology
Campus Mitte
Charitéplatz 1
10117 Berlin
Germany
friederike.irmen@charite.de

*these authors contributed equally to the manuscript

bioRxiv preprint doi: https://doi.org/10.1101/665976; this version posted June 10, 2019. The copyright holder for this preprint (which was not certified by peer review) is the author/funder. All rights reserved. No reuse allowed without permission.

Abstract

In Deep Brain Stimulation (DBS) of the subthalamic nucleus (STN) for treatment of Parkinson's Disease (PD), there is a paradigm shift away from focal stimulation of target structures toward effects of stimulation on distributed brain networks. While the relationship between modulated networks and *motor* outcomes has received much attention, network impact of *non-motor* DBS effects has been less well characterized. In the affective domain, STN-DBS improves depressive symptoms in some patients, while it leads to no change or even symptom-worsening in others. Here, we systematically investigate the impact of electrode placement and associated structural connectivity on changes in depressive symptoms following STN-DBS.

Depressive symptoms before and 6-12 months after STN-DBS surgery were documented in 116 PD patients from three DBS centers (Berlin, Queensland, Cologne). Individual electrode placements were reconstructed based on pre- and postoperative imaging using Lead-DBS software. Applying a finite element approach the volumes of tissue activated (VTA) were estimated and combined with normative connectome data to identify structural connections passing through VTAs. Berlin and Queensland data (N=80) were used for training and cross-validation to identify a structural connectivity profile that could explain improvement or worsening of depressive symptoms. The Cologne dataset (n=36) served as test-set for which depressive symptom change was predicted.

We identified a robust pattern linking structural connectivity to depressive symptoms under STN-DBS. An optimal connectivity map trained on the Berlin cohort could predict changes in depressive symptoms in Queensland patients ($R = 0.52$, $p < 0.0001$) and vice versa ($R = 0.57$, $p < 0.0001$). Furthermore, the joint training-set map predicted changes in depressive symptoms in the independent test-set from Cologne ($R = 0.36$, $p = 0.012$). Crucially, worsening of depressive symptoms was consistently associated with connectivity to left dorsolateral prefrontal areas, the prime target for non-invasive stimulation in depression. In contrast, depressive symptoms improved in patients with less connectivity to the left PFC. Results remained significant when controlling for motor improvement and dopaminergic medication withdrawal.

A specific structural connectivity profile implicating a left-lateralized prefrontal–STN network predicts depressive symptoms following STN-DBS: fibers linking the STN electrode with left prefrontal areas predicted worsening of depressive symptoms across DBS centers, cohorts and surgeons. Our results suggest that for the left STN-DBS lead, placement impacting fibers to left prefrontal areas should be avoided to maximise improvement of depressive symptoms. These findings pave the way toward personalized brain stimulation in which individual connectivity profiles and symptom constellations may determine optimal DBS targeting.

bioRxiv preprint doi: https://doi.org/10.1101/665976; this version posted June 10, 2019. The copyright holder for this preprint (which was not certified by peer review) is the author/funder. All rights reserved. No reuse allowed without permission.

Introduction

For a long time, it was assumed that deep brain stimulation (DBS) exerts its function via local modulation of target structures such as the subthalamic nucleus (STN), providing relief of motor symptoms in movement disorders such as Parkinson's disease (PD). Today, we experience a paradigm shift away from focal stimulation toward studying effects of DBS on distributed brain networks (Accolla *et al.*, 2016; Lozano & Lipsman, 2013). For example, a strong and robust relationship between connectivity profiles of DBS electrodes and clinical improvement has been shown in PD (Horn *et al.*, 2017a) and recently in patients with obsessive compulsive disorder (Baldermann *et al.*, 2019). A currently accepted theoretical framework postulates that DBS stimulation of basal ganglia targets may lead to changes in non-motor symptoms by modulating overlapping cortex-basal ganglia motor and non-motor loops (Haynes & Haber, 2013; Krack *et al.,* 2010). In PD, variable effects of DBS on non-motor traits have been described in various domains including autonomic function, sleep, cognition and mood (Chaudhuri & Schapira, 2009; Dafsari *et al.*, 2018a;2019; Fasano *et al.*, 2012; Kurtis *et al.*, 2017; Witt *et al.*, 2008;2012). In the affective domain, in addition to postoperative hypomania (Volkmann *et al.*, 2010), acute depression can also be a side effect of STN-DBS in PD patients (Funkiewiez *et al.*, 2006, 2003; Voon *et al.*, 2008) with a prevalence of about 20-25% (Witt *et al.*, 2012) despite slight improvement after 6 months (Weaver *et al.*, 2009; Witt *et al.*, 2008). Interestingly, STN-DBS has been reported to *improve* (Campbell *et al.*, 2012; Daniele *et al.*, 2003), *worsen* (Follett *et al.*, 2010; Temel *et al.*, 2006) or to have *no effect* (Deuschl *et al.*, 2006; Weaver *et al.*, 2009) on symptoms of depression or anxiety. However, unlike mania, postoperative depressive symptoms have rarely been associated with sensorimotor STN stimulation itself but rather with too fast tapering of dopaminergic medication (Thobois *et al.*, 2010) and stimulation of more ventral STN territory or even zona incerta stimulation (Bejjani *et al.*, 1999; Okun *et al.*, 2009; Witt *et al.*, 2012). Indeed, the precise local placement of DBS electrodes has an effect on non-motor DBS effects (Dafsari *et al.*, 2018b; Irmen *et al.*, 2019; Mallet *et al.*, 2007; Mosley *et al.*, 2018; Witt *et al.*, 2013) and modulation of distant brain regions involved in affective processing might play a crucial role on how affective symptoms develop after surgery.

In this study, we investigate the impact of electrode placement and associated structural connectivity on changes in depressive symptoms following STN-DBS. To this end, we reconstructed electrode placement in 80 PD patients from two international DBS centres and estimated their structural connectivity profiles. Based on these connectivity profiles, we

bioRxiv preprint doi: https://doi.org/10.1101/665976; this version posted June 10, 2019. The copyright holder for this preprint (which was not certified by peer review) is the author/funder. All rights reserved. No reuse allowed without permission.

calculated models that could explain and cross-predict worsening or improvement in depressive symptoms as measured with the Beck Depression Inventory- 2nd Edition (BDI-II; Beck *et al.*, 1996). Finally, we validated these models using a testing set of 36 PD patients form a third DBS centre.

Materials and methods

Patient cohorts and imaging

A total of 121 patients from three DBS centers (Berlin [BER]: n = 32; Queensland [QU]: n = 49; Cologne [CGN]: n = 40) were included in this retrospective study (age 62 ± 0.84 years, 43 women). Data from Charité Universitätsmedizin Berlin and University of Queensland were used to form the *training* and *cross-validation datasets* to identify structural connectivity predicting mood changes after DBS surgery. Data from the University Hospital Cologne was used as a *test dataset* to validate the established model. Five patients were excluded from the analyses for the following reasons: One patient (QU) due to incomplete data, two patients (CGN) due to unilateral VIM (instead of STN) stimulation, and two patients (CGN) due to clinically relevant psychiatric symptoms before surgery that were pharmacologically treated. The sample characteristics of the final cohort (n = 116) are presented in Table 1. Detailed descriptions of all patients are listed in Supplementary Table 1.

All patients underwent stereotactic DBS surgery for treatment of PD and received bilateral DBS electrodes (n = 42 model 3389 Medtronic, Minneapolis, MN; n = 31 Boston Scientific Vercise; n = 36 Boston Scientific Vercise Cartesia Directional; n = 7 St Jude Infinity Directional model 6172). Structural abnormalities were excluded using preoperative MRI. Clinically-significant psychiatric symptomatology and cognitive deficits (defined as deficient performance in Mini-Mental State Examination score or multidomain deficits in neuropsychological tests such as features of PD dementia; Emre et al., 2007) were excluded prior to DBS by psychiatric evaluation and neuropsychological testing. Lead placement was validated using microelectrode recordings during surgery (BER, QU, CGN), intraoperative macrostimulation (BER, QU, CGN) and postoperative imaging (BER, QU, CGN). Depressive symptoms were recorded pre- and postoperatively (after 7.56 ± 2.9 months, when DBS settings had already been titrated intensively and stable settings have been reached) using BDI-II (cut-off values 0-13: minimal depression; 14-19: mild depression; 20-28: moderate depression; >29: severe depression). Furthermore, levodopa equivalent daily dosage (LEDD) and Unified Parkinson's Disease Rating Scale Part III (UPDRS-III) ON medication were recorded preoperatively and

bioRxiv preprint doi: https://doi.org/10.1101/665976; this version posted June 10, 2019. The copyright holder for this preprint (which was not certified by peer review) is the author/funder. All rights reserved. No reuse allowed without permission.

postoperatively ON DBS in all patients and included in the analysis as covariates. Clinical data were compared pre- and postoperatively using randomized permutation tests (5000 permutations) to test for significance ($p<0.05$ considered significant). The study was approved by the local ethics committee at each site and carried out in accordance with the Declaration of Helsinki.

Localization of DBS electrodes

DBS electrodes were localized using the Lead-DBS toolbox (www.lead-dbs.org; Horn & Kühn, 2015). Specifically, the advanced processing pipeline illustrated in Horn *et al.* (2019) was applied (Horn *et al.*, 2019a). In short, postoperative CT or MRI were linearly coregistered to preoperative MRI using advanced normalization tools (ANTs; stnava.github.io/ANTs/; Avants *et al.*, 2008). Coregistrations were visually inspected and refined if needed. A brainshift correction step was applied as implemented in Lead-DBS. All preoperative volumes were used to estimate a precise multispectral normalization to ICBM 2009b NLIN asymmetric ("MNI") space applying the ANTs SyN Diffeomorphic Mapping method (Avants *et al.*, 2008) using the preset "effective: low variance default + subcortical refinement" implemented in Lead-DBS. In some patients where this strategy failed, a multispectral implementation of the Unified Segmentation approach (Ashburner & Friston, 2005) implemented in Statistical Parametric Mapping software (SPM12; http://www.fil.ion.ucl.ac.uk/spm) was applied. These two methods are available as presets in Lead-DBS and were top-performers to segment the STN with precision comparable to manual expert segmentations in a recent comparative study (Ewert *et al.*, 2019). DBS contacts were automatically pre-reconstructed using PaCER (Husch *et al.*, 2018) or the TRAC/CORE approach (Horn & Kühn, 2015) and manually refined if needed. For segmented leads, the orientation of electrode segments was reconstructed using the Directional Orientation Detection (DiODe) algorithm (Hellerbach *et al.*, 2018; Sitz *et al.*, 2017).

Volume of Tissue Activated and connectivity estimation

The volume of tissue activated (VTA) was calculated using default settings in Lead-DBS applying a Finite Element Method (FEM) -based model (Horn *et al.*, 2017a). This model estimates the E-field (i.e. the gradient distribution of the electrical charge in space measured in volt per millimeter) on a tetrahedral mesh that differentiates four compartments (grey and white matter, electrode contacts and insulation). Grey matter was defined by key structures (STN, internal and external pallidum, red nucleus) of the DISTAL atlas (Ewert *et al.* 2017). The

bioRxiv preprint doi: https://doi.org/10.1101/665976; this version posted June 10, 2019. The copyright holder for this preprint (which was not certified by peer review) is the author/funder. All rights reserved. No reuse allowed without permission.

resulting gradient vector magnitude was thresholded at a heuristic value of 0.2 V/mm to generate the VTA.

Recently, it has been shown that using binarized VTAs (that would model all-or-nothing activations) could predict slightly less variance in clinical outcomes in comparison to using weighted VTAs such as the E-field gradient vector magnitudes (Horn *et al.*, 2019). Binary VTAs are based on specific thresholds that assume a certain type of axon diameter and orientation and do not grasp the anatomical complexity of the subcortex (e.g. Forstmann *et al.*, 2016). To account for this general limitation of the VTA concept, we repeated all analyses using the unthresholded E-field magnitude instead of the VTAs surrounding the active electrode contacts for the connectivity analysis (see Horn *et al.*, 2019 for details).

Whole-brain structural connectivity profiles seeding from bilateral VTAs or E-Fields were estimated using a Parkinson's Disease group connectome that is based on publicly available data (Marek *et al.*, 2011; Parkinson's Progression Markers Initiative; www.ppmi-info.org). This PPMI normative connectome of PD patients (age n = 90; age 61.38 ± 10.42, 28 female) was priorly computed (Ewert *et al.*, 2017) and has been used in context of DBS multiple times before (Horn *et al.*, 2017a, 2017b, 2019; Neumann *et al.*, 2018). For each patient, fibers that passed through the VTA or a non-zero voxel of the E-Field were selected from this normative connectome and projected onto a voxelized volume in standard space (1mm isotropic resolution) while keeping count of the fibers traversing each voxel. In the binary (VTA) analyses, the number of fibres traversing each voxel were denoted (resulting in classical fibre-density map), in the E-Field based analyses, each fibre received the weight of the maximal E-Field magnitude of its passage and fibre densities were weighted by these values. Figure 1 provides an overview over the methodology applied.

bioRxiv preprint doi: https://doi.org/10.1101/665976; this version posted June 10, 2019. The copyright holder for this preprint (which was not certified by peer review) is the author/funder. All rights reserved. No reuse allowed without permission.

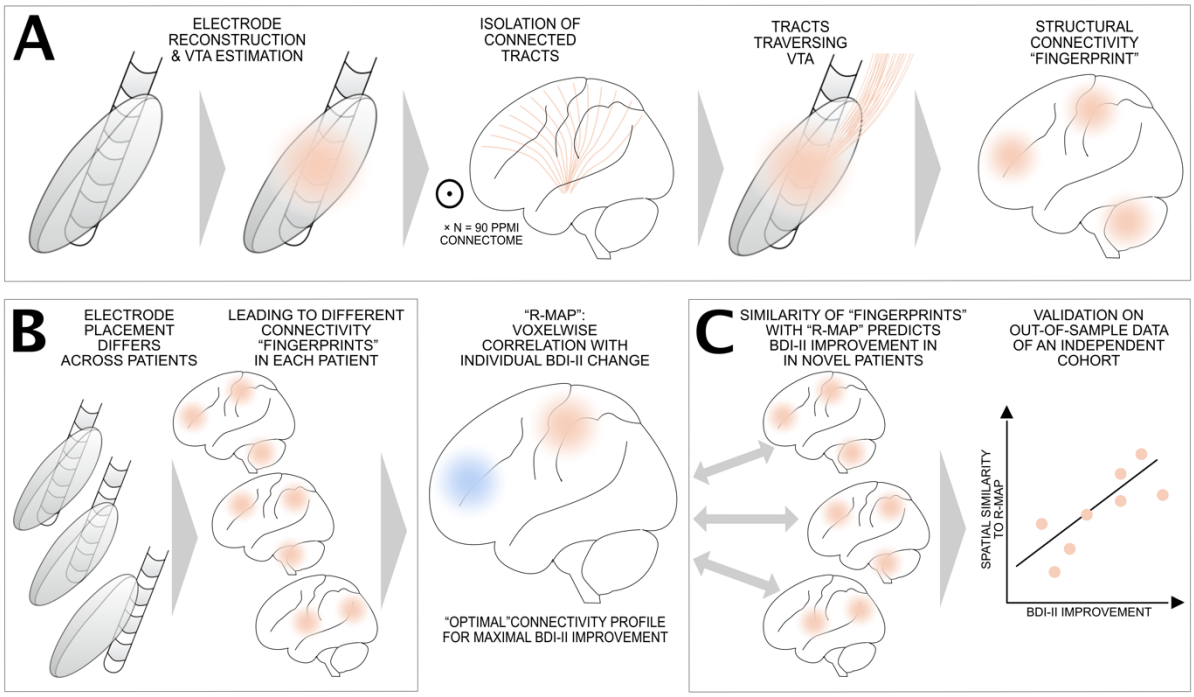

Figure 1: Overview of applied methods. A) In each patient, electrodes were localized and VTAs were calculated in standard stereotactic space using Lead-DBS software. From a normative Parkinson's Disease connectome (N = 90 PPMI datasets), tracts that traversed through each patient's VTA were selected and projected to the brain as fiber density maps. These maps represent the structural connectivity "fingerprint" seeding from each VTA. B) Varying electrode placement leads to different connectivity "fingerprints" in each patient. Across the group of patients, these fingerprints are used to generate a model of connectivity that is associated with maximal BDI-II improvement by voxel-wise correlation ("R-Map"). C) The R-Map represents a model that denotes how electrodes should be connected to result in maximal BDI-II improvement. When comparing each novel patient's "fingerprint" with this model (by means of spatial correlation), individual BDI-II improvement can be predicted. Crucially, this is done to predict improvement in out-of-sample data, i.e. across cohorts or in a leave-one-out fashion throughout the manuscript. This means that the R-map is never informed by the predicted patient's structural connectivity "fingerprint".

Modelling connectivity-driven mood changes

Structural connectivity strength, i.e. the number of fibers between VTA and each voxel was Spearman rank-correlated with BDI-II change (preoperative - postoperative), which resulted in a connectivity map that shows positive or negative associations with BDI-II improvement. In the following, these types of maps are referred to as R-maps (since they denote Spearman's correlation coefficients for each voxel). Spearman's correlation was used since tractography results are highly non-Gaussian distributed and rather follow an exponential distribution (e.g. Horn *et al.*, 2014). All analyses were carried out in Matlab (The Mathworks, Natwick, MA). We used randomized permutation tests (5000 permutations) to test for significance (at a 5% significance level) and used Spearman's correlation coefficients throughout all analyses.

bioRxiv preprint doi: https://doi.org/10.1101/665976; this version posted June 10, 2019. The copyright holder for this preprint (which was not certified by peer review) is the author/funder. All rights reserved. No reuse allowed without permission.

Validation of the training dataset. One R-map for each subset (BER, QU) was calculated. R-maps were then used to predict BDI-II changes in out-of-sample data (i.e. cross-predicting between QU ↔ BER cohorts) by spatial correlation between the R-map (model) and the connectivity profile seeding from the VTAs in each patient. This was done across voxels with an absolute Spearman's R-value of > 0.1 on each R-map. For example, the R-map (model) was calculated across the BER sample and voxels with an absolute R > 0.1 were spatially correlated with connectivity maps in the QU sample. For each patient in the QU cohort, this led to one R-value that coded for spatial similarity to the model. These R-values were then correlated with empirical BDI-II changes. An additional leave-one-out cross-validation (i.e. data from patients 1-79 was used to predict patient 80 and so on) across the training sample (BER/QU combined) was run to test whether similarity to the specific structural connectivity profile of the training set (which is denoted by the R-map) could significantly predict absolute BDI-II change. Furthermore, we validated the results by running the analyses again based on the E-field instead of VTA; using the percentage BDI-II change relative to baseline instead of the absolute BDi change. Moreover, to test for potential lateralization of connectivity profile, we reran analyses for left and right VTAs separately.

Prediction of the test dataset. In the same fashion as the cross-prediction between the subcohort of the training dataset, a joint R-map for the entire training/cross-validation set (BER+QU) was generated, which was used to predict data BDI-II change in patients of the test dataset (CGN).

Testing robustness of the model across the entire sample. We applied the leave-one-out cross-validation across the whole dataset, i.e. data from patients 1-115 was used to predict patient 116 and so on. Finally, to control for the effect of postoperative LEDD and UPDRS-III reduction, those variables were included in the prediction models as covariates.

Isolation of fibertracts that are discriminative for mood changes

In an additional analysis, we sought to identify tracts that could discriminate patients with positive from negative BDI-II change. For each fibertract in the normative connectome (PPMI 90, see above), its accumulative E-Field vector magnitude while passing by each patient's electrode was denoted. This value was then Spearman rank-correlated with each patient's clinical change in depressive symptoms. Thus, a fibertract that passed close to active contacts of patients that had BDI-II improvement but far from active contacts in patients that had BDI-II worsening would receive a high Spearman's R value (and tracts exhibiting the inverse property received a highly negative R value). These R values were used to color-code fibertracts that were positively and negatively predictive of BDI-II improvement. This analysis was

bioRxiv preprint doi: https://doi.org/10.1101/665976; this version posted June 10, 2019. The copyright holder for this preprint (which was not certified by peer review) is the author/funder. All rights reserved. No reuse allowed without permission.

expected to show identical (or highly similar results) as the "R-map" method explained above but with the advantage of working on a tract-by-tract basis (instead of a voxel-wise fashion). Thus, it is ideal to visualize the actual fibertracts that were predictive of change in depressive symptoms. Given the similarity of the methodology, this analysis was only performed once on the complete set of patients to further characterize the tracts that are likely responsible for BDI-II changes under STN-DBS. The fibertract analysis was validated across the whole data set with a leave-one-cohort-out cross-prediction, which predicted data of any one of the three DBS centres by data of the two other centers following the procedure of Li et al., 2019.

Results

Clinical data

Disease duration in the entire sample (n = 116; Table 1; Supplementary Table 1 for more details) was 9.55 ±4.45 years. DBS lead placement was similar across all three cohorts (Figure 2A,3C). Motor improvement with DBS was significant although we measured it ON medication reaching an average DBS response of 27.56 ±8.37 % (i.e. M ±SEM throughout the paper) as measured by the UPDRS-III. Preoperative LEDD was 1142.46mg ±52.69 as compared to postoperative 464.45mg ±27.05 (56.55 ±2.77 % reduction) with a contribution of dopamine agonists (DA) of 191.06mg ±16.62 pre- and 107.51mg ±10.73 postoperatively. Total LEDD, LEDD of DA, and UPDRS-III reduction were not significantly different in training and test datasets ($p > 0.05$ for all three variables, see table 1 for mean values). On average, BDI-II scores decreased from 9.94 ±0.50 to 8.96 ±0.60 (on average by 0.97 ±0.54 points = absolute BDI-II change) postoperatively, i.e. there was an overall reduction in BDI-II of 3.34 ± 8.12% but the difference was not significant. Importantly, scores in some patients improved while others worsened (with an absolute BDI-II change in single patients – of up to 19, Supplement 1). In the test dataset (Supplementary Table 1 – Cologne), some specific features were noted: patient #10 and #19 were diagnosed with comorbid depression and anxiety disorder at baseline; patient #13 reported pain and relatedly negative mood. Those three patients are marked with asterisk in Figure 3B.

bioRxiv preprint doi: https://doi.org/10.1101/665976; this version posted June 10, 2019. The copyright holder for this preprint (which was not certified by peer review) is the author/funder. All rights reserved. No reuse allowed without permission.

COHORT	N	AGE (YRS)		SEX		DISEASE DURATION (YRS)		MONTHS POST SURGERY	BDI-II (BASELINE)		BDI-II (POSTOP)		UPDRS-III (BASELINE, MED ON)		UPDRS-III (ON DBS, MED ON)		LEDD-REDUCTION (%)	
		M	*SEM*	*f*	*m*	*M*	*SEM*	*M*	*M*	*SEM*	*M*	*SEM*	*M*	*SEM*	*M*	*SEM*	*M*	*SEM*
BERLIN	32	61	2	10	22	10	1	12	11.56	1.11	11.56	1.32	20.78	1.82	19.26	2.47	46.06*	7.32
QUEENSLAND	48	62	1	15	33	8	1	6	11.06	0.68	8.45*	0.82	37.46	2.23	33.95	1.89	68.98*	3.32
COLOGNE	36	62	8	18	18	10	1	6	7.00	0.71	7.00	0.97	18.00	1.65	17.00	1.53	48.27*	3.15
TOTAL	116	62	1	43	73	9	0	7	9.94	0.50	8.96	0.60	26.75	1.43	24.85	1.35	56.32*	2.77

Table 1: Sample characteristics. BDI-II – Delta change in Beck's depression inventory (Baseline = pre; Postop = post DBS surgery); UPDRS-III –Unified Parkinson's disease rating scale III (Baseline = pre; Postop = post DBS surgery ON Medication); LEDD – Levodopa-equivalent daily dosage; M – mean; SEM – Standard error of the mean; *significant change compared to baseline

Connectivity related to DBS-induced mood changes

We identified a VTA-based structural connectivity map (R-map) predictive of postoperative BDI-II change in the training dataset (Figure 3A). The more fibers connected a patient's VTA to the positive areas (warm colors) of this map, the more their depressive symptoms improved postoperatively. On the contrary, the more a patient's VTA was structurally connected to the negative areas (cold colors) of this map, the more their depressive symptoms worsened postoperatively.

Validation of the training dataset. The R-maps of the two subcohorts in the training dataset were similar: On the right hemisphere of the R-map, connectivity to motor and prefrontal regions is universally associated with depressive symptom improvement. On the left hemisphere however, connectivity to the prefrontal cortex (PFC), including the dorsolateral PFC is strongly associated with worsening of depressive symptoms, whereas connectivity to sensorimotor and superior parietal areas is associated with symptom improvement (Figure 2). Cross-predictions were significant, i.e. the R-map based on BER-data could predict BDI-II change in relation to structural connectivity in the QU dataset (Figure 2C, $R = 0.52$, $p < 0.0001$) and vice versa ($R = 0.57$, $p < 0.0001$). In a leave-one-out cross-validation across the training sample (BER/QU combined), similarity to this specific structural connectivity profile (which is denoted by the R-map) could significantly predict absolute BDI-II change ($R = 0.26$, $p = 0.01$) even when basing structural connectivity profiles on the E-field instead of VTA ($R = 0.24$, $p = 0.015$) or when using the percentage BDI-II change relative to baseline ($R = 0.20$, $p = 0.04$). To test whether the effect was lateralized to either hemisphere, we reran analyses for left and right VTAs separately and found that connectivity on either hemisphere alone was predictive for BDI-II change as well (right: $R = 0.347$, $p = 0.002$; left: $R = 0.359$, $p = 0.001$).

Prediction of the test dataset. The R-map based on the whole training set (BER/QU combined) was used to predict BDI-II change in the independent test dataset (CGN) by calculating spatial

bioRxiv preprint doi: https://doi.org/10.1101/665976; this version posted June 10, 2019. The copyright holder for this preprint (which was not certified by peer review) is the author/funder. All rights reserved. No reuse allowed without permission.

similarity between each CGN-patient's electrode connectivity profile with the BER/QU R-map. This could again validate our results and a significant correlation was observed (Figure 3B, $R = 0.36$, $p = 0.012$).

Testing robustness of the model across the entire sample. Although the CGN cohort was kept isolated from data-analysis until this very last step, we opted to create one final R-map across all available data to calculate a final connectivity profile that codes for BDI-II change based on all information present. This final connectivity map predictive for BDI-II change in all three cohorts (n = 116) is displayed in Figure 4A. To further validate robustness of this final R-map, we performed one last leave-one-out cross validation analysis (Figure 4B, $R = 0.33$, $p < 0.001$). Moreover, this prediction model remained significant when including postoperative LEDD reduction, reduction of dopamine agonists and percentage UPDRS-III change (postoperative – preoperative) as additional covariates and correcting for cohort in a joint general linear model ($R^2 = 0.21$, $F_{(112,105)} = 4.78$, $p = 0.0002$). Thus, this final model was able to explain 21% of variance in BDI-II change based on clinical covariates and structural connectivity profiles across the whole group of subjects.

Fibertracts related to mood changes

An additional analysis was run to identify the actual tracts (instead of their cortical projection sites) that were correlated with BDI-II improvement when modulated. This was done on a tract-by-tract instead of voxel-wise basis but further confirmed our results using a different analysis pathway. Crucially, this data-driven analysis revealed largely more tracts on the left hemisphere than on the right hemisphere, again suggesting an impact of left DBS stimulation on change of depressive symptoms (Figure 5A). Using lower thresholds, the pattern was similar between the two hemispheres but left hemispheric tracts were more predictive of BDI-II change and predictive tracts were found in larger quantities. The analysis revealed that the positively and negatively associated tracts seemed to differ in their anatomical course in that the negatively associated tract passed by the STN medial and at level of its limbic/associative functional zone, while the positively correlated tract passed through and slightly lateral to the motor STN (Figure 5B). Moreover, as can be seen in Figure 5C, the negatively associated tract traverses more laterally when ascending to the PFC. Robustness of this tract was validated using leave-one-cohort-out crossvalidations which supported the results from our R-map model: any of the cohorts could be predicted by the other two cohorts (BER/QU predicting CGN; QU/CGN predicting BER; BER/CGN predicting QU) $R = 0.24$, $p = 0.001$.

bioRxiv preprint doi: https://doi.org/10.1101/665976; this version posted June 10, 2019. The copyright holder for this preprint (which was not certified by peer review) is the author/funder. All rights reserved. No reuse allowed without permission.

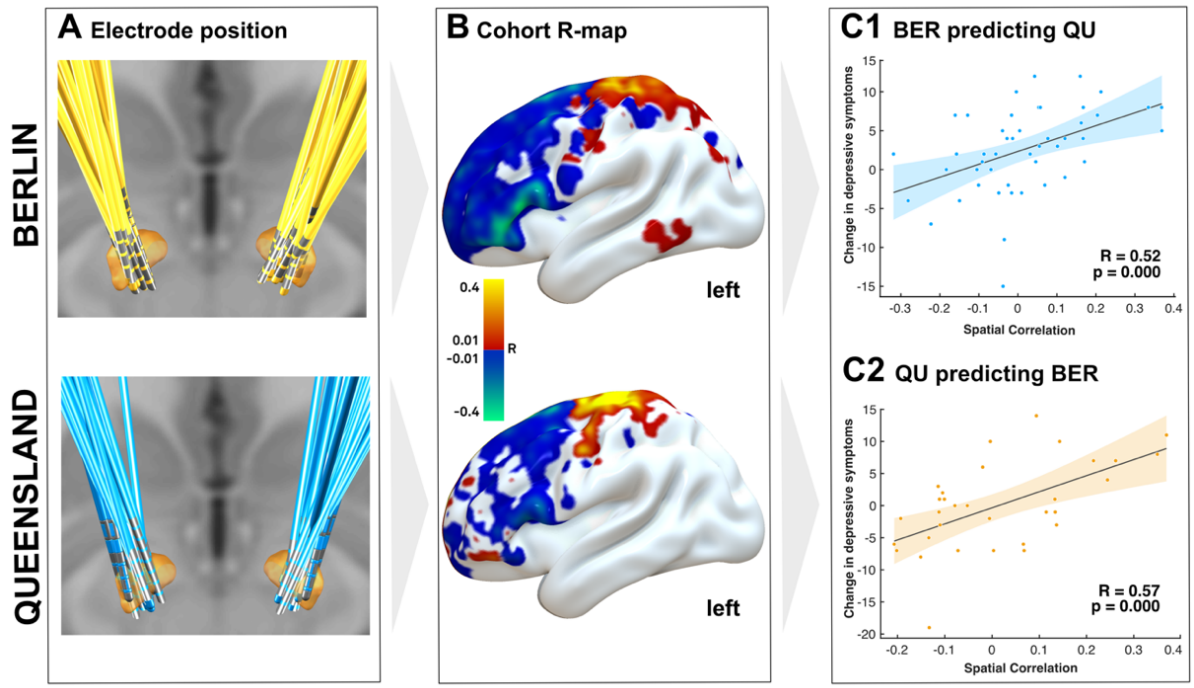

Figure 2: Structural connectivity predicting change in depressive symptoms in the training dataset (N = 80). A) Electrode position for the two cohorts from Berlin and Queensland. B) Each cohort's R-Map represents the association with change in depressive symptoms under STN-DBS. Negative (blue) areas of the left hemisphere shown here relate to worsening of depressive symptoms. R-Maps revealed a significant association between worsening of depressive symptoms after STN-DBS and connectivity to left dorsolateral PFC. C1) Based on the R-Map from the Berlin cohort, depressive symptoms in the Queensland Cohort could be significantly predicted and vice versa (C2). R-Maps are presented smoothed with a 3mm full-width half-maximum Gaussian kernel to increase signal-to-noise ratio.

bioRxiv preprint doi: https://doi.org/10.1101/665976; this version posted June 10, 2019. The copyright holder for this preprint (which was not certified by peer review) is the author/funder. All rights reserved. No reuse allowed without permission.

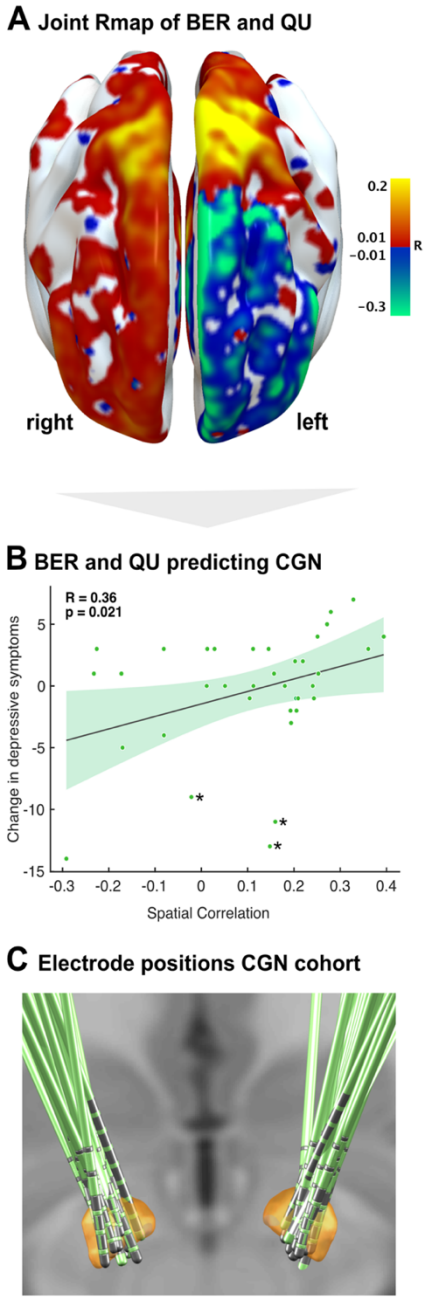

Figure 3: R-map of the training-dataset and prediction of the test-dataset. A) R-Map of the training dataset. Negative (blue) areas represent association with worsening of depressive symptoms while positive (red) areas represent association with improvement of depressive symptoms under STN-DBS. The R-Map is presented smoothed with a 3mm full-width half-maximum Gaussian kernel to increase signal-to-noise ratio. B) The R-Map of the training dataset (Berlin-Queensland model) significantly predicted change in depressive symptoms in the test-dataset (Cologne). Patients marked with asterisks showed moderate worsening in depressive symptoms with comorbidities and pain, which remained stable over the period of assessment; hence patients were not excluded from the test dataset. C) Electrode positions of the test dataset within the STN.

bioRxiv preprint doi: https://doi.org/10.1101/665976; this version posted June 10, 2019. The copyright holder for this preprint (which was not certified by peer review) is the author/funder. All rights reserved. No reuse allowed without permission.

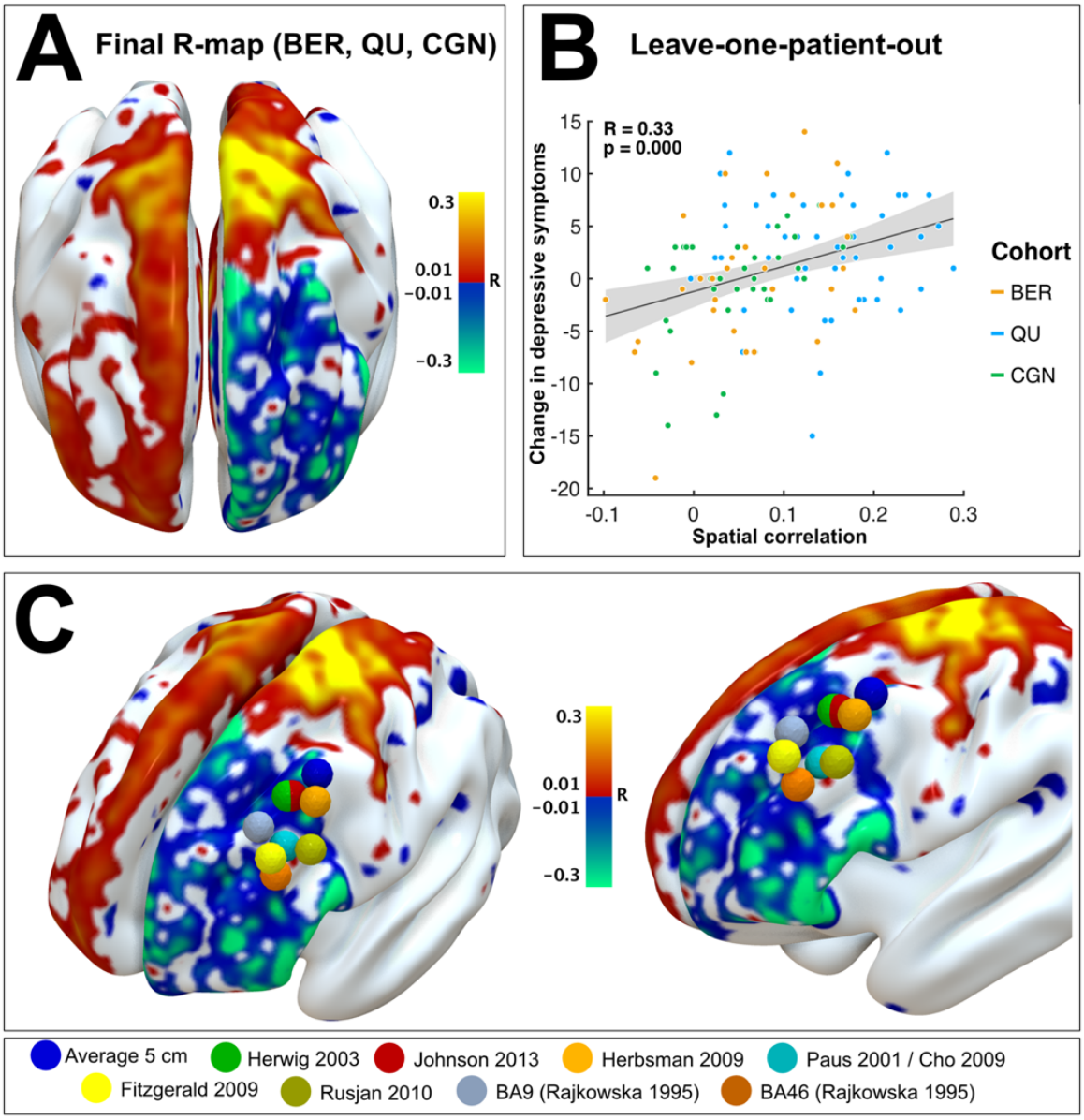

Figure 4: Final R-Map validation across all patients and proximity to TMS targets. A) R-Map associated with change of depressive symptoms over all patients (n = 116). B) Validation of the model using the approach of leaving-one-out design. C) rTMS targets for treatment of depression superimposed on final R-Map. R-Maps are presented smoothed with a 3mm full-width half-maximum Gaussian kernel to increase signal-to-noise ratio.

bioRxiv preprint doi: https://doi.org/10.1101/665976; this version posted June 10, 2019. The copyright holder for this preprint (which was not certified by peer review) is the author/funder. All rights reserved. No reuse allowed without permission.

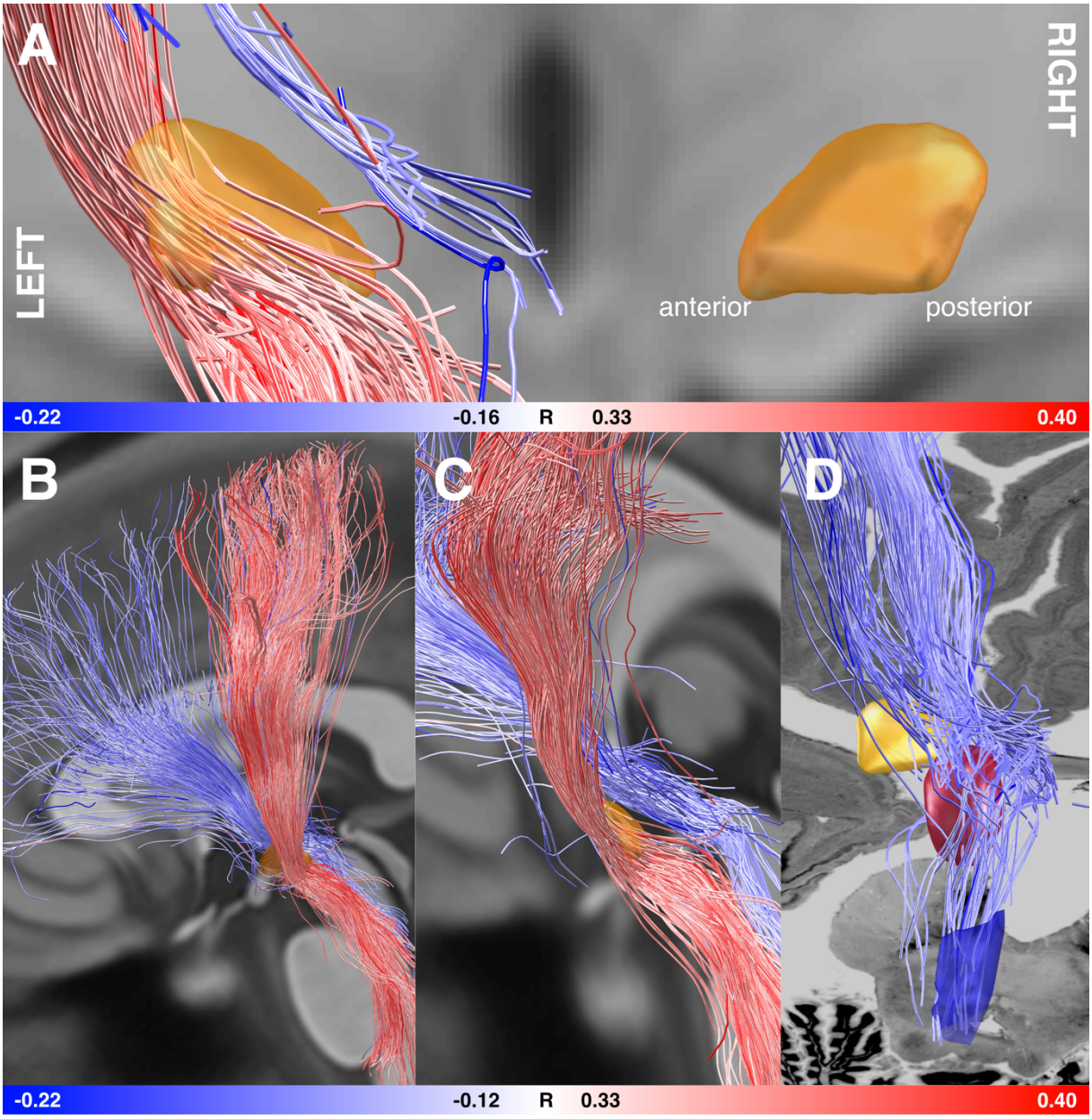

Figure 5: Fibertracts discriminative of BDI-II improvement when modulated. Red tracts are positively, blue tracts negatively correlated with clinical improvement. STN shown in orange. A) Coronal view from posterior with both hemispheres. At this threshold level, no fibers on the right hemisphere were associated with clinical improvement but a strong set of both positive and negative fibers were found on the left hemisphere. B) View from the left and C) view parallel to the longitudinal axis of the left STN. Positively and negatively correlated fibertracts seem to be distinct tracts, the positive one passing through the STN and lateral to it, the negative one medial and anteriorly. D) Superimposed on a section of the BigBrain ultrahigh resolution human brain model (Amunts *et al.*, 2013), at the level of the brainstem, the negative tract seems to traverse around the red nucleus and may connect to (or originate from) brainstem nuclei such as the left dorsal raphe nucleus (shown in dark blue as defined by the Harvard Ascending Arousal Network Atlas; (Edlow *et al.*, 2012)).

bioRxiv preprint doi: https://doi.org/10.1101/665976; this version posted June 10, 2019. The copyright holder for this preprint (which was not certified by peer review) is the author/funder. All rights reserved. No reuse allowed without permission.

Discussion

In this study, we modelled structural connectivity predictive for changes in depressive symptoms following STN-DBS. We identified a robust connectivity pattern linking worsening of depressive symptoms to left prefrontal impact. Three main conclusions can be drawn from these results. First, a distinct VTA-based structural connectivity profile can predict long-term change in depressive symptoms associated with STN-DBS in PD patients. Second, the connectivity profile is robust and able to predict data across cohorts and in an independent test sample. Third, left-hemispheric negative connectivity to the PFC predicting less benefit of DBS on depressive symptoms in our cohort may suggest that anteromedial fibers to left prefrontal areas should be avoided for left STN-DBS lead placement to maximise improvement of depressive symptoms.

A common assumption in clinical research on affective changes associated with STN-DBS is that they result from rapid withdrawal of dopaminergic replacement therapy after surgery (Thobois *et al.*, 2010) increasing anhedonia induced through dysregulation in affective networks (Belujon & Grace, 2017; Dunlop & Nemeroff, 2007). While this is an important factor explaining acute and subacute postoperative affective changes, in our large multi-center sample using long-term data, LEDD reduction did not explain BDI-II change. Perhaps this relates to clinicians addressing this potential risk-factor for depression during long-term follow up. Others have also reported a lack of correlation between LEDD reduction and non-motor PD symptoms like apathy and mood (Dafsari *et al.*, 2018; Dafsari *et al.*, 2018b). Yet, the general notion is that STN-DBS mimics the action of dopaminergic agents (Volkmann *et al.*, 2010) and acute stimulation more likely leads to hypomania as depression (Appleby *et al.,* 2007; Castrioto *et al.*, 2014; Funkiewiez *et al.*, 2003; Krack *et al.*, 2010; Romito *et al.*, 2002; Volkmann *et al.*, 2010; Witt *et al.*, 2008) potentially relating to stimulation of contacts in the anterior, ventral and medial planes (Chopra et al., 2011). Interestingly, long-term improvement in motor symptoms as measured with UPDRS-III did not add to the explanation of BDI-II change by connectivity in our sample, suggesting that stimulation may influence affective processing more directly, i.e. via connectivity to limbic/prefrontal areas.

The association of depressive symptoms and connectivity to the left PFC is not surprising given the vast amount of evidence linking depression to left frontal lesions. Specifically, hypoactivity and dysfunction of the left PFC is commonly found in patients with depression (Chang *et al.*, 2011; Grimm *et al.*, 2007; Hamilton *et al.*, 2012; Koenigs *et al.*, 2008; Mayberg *et al.*, 2005; Thomas *et al.*, 2003) and there is an increase of depressive symptoms after left dlPFC traumatic

bioRxiv preprint doi: https://doi.org/10.1101/665976; this version posted June 10, 2019. The copyright holder for this preprint (which was not certified by peer review) is the author/funder. All rights reserved. No reuse allowed without permission.

brain injury (Fedorof *et al.*, 1992; Jorge *et al.*, 2004; Leung *et al.*, 2018) and stroke (Egorova *et al.*, 2017; Grajny *et al.*, 2016; Hama *et al.*, 2007; Shi *et al.*, 2017). In particular, Grainy *et al.* (2016) found that severity of depression is directly related to the extent of dlPFC damage suggesting gradual impact of frontal damage on networks underlying depressive symptoms. Indeed, large-scale network effects, hemispheric asymmetries and connectivity play an important role in the development of depressive symptoms; e.g. post-stroke depression has been linked to altered functional connectivity of dlPFC to the frontoparietal cognitive control network (Egorova *et al.*, 2017) and dlPFC connectivity in general plays a major role in depression (Hwang *et al.*, 2015; Kaiser *et al.*, 2015; Sheline *et al.*, 2010). In particular, the left dlPFC seems to be regulating negative affect through reappraisal and voluntary suppression (Koenigs *et al.*, 2010; Lévesque *et al.*, 2003; Ochsner *et al.*, 2004; Phan *et al.*, 2005) via the frontoparietal cognitive control network (Pan *et al.*, 2018). In patients suffering from major depression, excitability of the hypoactive dlPFC tissue (Chang *et al.*, 2011; Grimm *et al.*, 2007; Hamilton *et al.*, 2012; Koenigs *et al.*, 2008; Mayberg *et al.*, 2005; Thomas *et al.*, 2003) has been augmented with non-invasive brain stimulation using high-frequency repetitive transcranial magnet stimulation (rTMS) leading to symptom amelioration (Pascual-Leone *et al.*, 1996). Although the precise mechanism of dlPFC rTMS in improving depressive symptoms is not yet fully understood, a role of local and remote network changes and altered connectivity of prefrontal structures is evident (Fox *et al.*, 2012, 2013; Philip *et al.*, 2018). Interestingly, the common targets of rTMS in depression that have been summarized by Fox *et al.* (2013) precisely lie within the clusters we find negatively associated with BDI-II improvement under STN-DBS; Figure 4C). Thus, when depressive symptoms worsen under long-term STN-DBS, the VTAs are tempering fibers linked to the left dlPFC.

When asking why structural connectivity from VTAs to the left dlPFC explains depressive symptom change, several aspects should be considered. First, a correlation of fibertracts with BDI-II change clearly shows that worsening of depressive symptoms under STN-DBS is associated with fibers connecting prefrontal areas via zona incerta to the dorsal mesencephalon and brainstem (Figure 5). We presume that STN-DBS may disrupt information flow along these connecting fibers between prefrontal areas and the brainstem. One candidate brainstem region whose link to the PFC might be disturbed by DBS leading to depression is the dorsal raphe nucleus (DRN), which is part of the serotonergic system that is known to impact mood states (Michelsen *et al.* , 2008; Politis *et al.*, 2010; Wei *et al.*, 2018) and which is hypoactive in depression (Michelsen *et al.*, 2007). Indeed, unbalanced connectivity of the DRN and prefrontal areas is related to depression (Ikuta *et al.*, 2017) and abnormal serotonergic neurotransmission

bioRxiv preprint doi: https://doi.org/10.1101/665976; this version posted June 10, 2019. The copyright holder for this preprint (which was not certified by peer review) is the author/funder. All rights reserved. No reuse allowed without permission.

has been – albeit inconsistently – linked with depression in PD (Politis *et al.*, 2010; Qamhawi *et al.*, 2015). Moreover, rodent studies have shown that STN-DBS may inhibit serotonergic output from the DRN (Hartung *et al.*, 2011) and that this induces depressive-like behavior (Tan *et al.,* 2011; Temel *et al.*, 2007). Since there are no direct connections between the STN and the DRN (Peyron *et al.*, 1997), one of the candidate neural pathways underlying the serotonergic suppression effect of STN-DBS is prefrontal-DRN connectivity (Tan *et al.*, 2011). Indeed, excitatory input from (medial) prefrontal areas directly modulates activity of serotonergic neurons in the DRN (Hajós *et al.*, 1998; Varga *et al.*, 2001;2003). Thus, accidental disruption of the serotonergic communication between left PFC and DRN may be a likely pathophysiological candidate to foster depressive states after STN-DBS. Another candidate neural substrate for the reported change in depressive symptoms is the ventral tegmental area, which as the origin of the meso-cortico-limbic dopamine projections is pivotal for reward-processing but also plays a role in depression (Wei *et al.*, 2018; Wohlschläger *et al.*, 2018). Yet, this neural substrate is less likely given the exact anatomical course of the tract.

Second, it is worth mentioning that like the striatum, the STN is a node of convergence of affective, cognitive and motor input (Accolla *et al.*, 2016; Alexander & Crutcher, 1990; Aron *et al.*, 2016; Haynes & Haber, 2013; Péron *et al.*, 2013; Sieger *et al.*, 2015). Its activity is modulated through coupling with PFC activity (Cavanagh *et al.*, 2011; Frank *et al.*, 2007; Herz, Zavala, Bogacz, & Brown, 2016) and, crucially, STN-DBS impacts affective processing (e.g. Irmen *et al.*, 2017; Péron *et al.*, 2010). Therefore, although here we see activation of fibertracts associated with BDI-II change passing medially by the STN, a role of the structure in affective processing and emotion regulation is undisputed (Campbell *et al.*, 2008; Mallet *et al.*, 2007; Péron *et al.*, 2015). Importantly, in our data, depressive symptoms improved if predominantly fibers connecting the dorsolateral (motor) STN to the motor cortex were stimulated as has been reported before (Eisenstein *et al.*, 2014). This implicates the overlapping presence of neurons involved in affective/associative processing and motor processing in the STN motor segment (Accolla *et al.*, 2017; Haynes & Haber, 2013; Irmen *et al.*, 2019). In turn, as a secondary effect, STN-DBS may impact subcortical-cortical structural connections by changing integration of balanced input from cognitive, affective and motor loops in the basal ganglia and related networks (Accolla *et al.*, 2014, 2016; Haynes & Haber, 2013; Irmen *et al.*, 2019; Rodriguez-Oroz *et al.*, 2011). The left-hemispheric laterality of the observed effect might however be specific to depression since other studies stressed the role of the right STN in the processing of positive emotional voices (Eitan et al., 2013) and stimulation of the right STN is associated with neuropsychiatric symptoms such as disinhibition (Mosley et al., 2018). These results are

bioRxiv preprint doi: https://doi.org/10.1101/665976; this version posted June 10, 2019. The copyright holder for this preprint (which was not certified by peer review) is the author/funder. All rights reserved. No reuse allowed without permission.

not mutually exclusive with our findings since they differ in their approach (network vs. local target anatomy and physiology). Effects of STN-DBS on cognition and affect are complex and we are only starting to understand the associated local, network, and physiological changes.

Taken together, in the left hemisphere, high-frequency stimulation of fibers anteromedial to the STN is associated with worsening of depressive symptoms while stimulation of dorsolateral STN leads to improvement of depressive symptoms in PD patients. The connectivity profile described in this study may be used to inform surgeons and clinicians in the placement and settings of STN-DBS, depending on the patient's individual connectivity that could be studied before surgery. Certainly, more work is needed to refine our understanding of the functionality of prefrontal to STN connectivity and the left-lateralized hemispheric impact; but this study introduces a new direction of avoiding harmful side effects of STN-DBS in PD patients by considering connectivity to networks guiding these side effects.

As a final consideration, it is important to stress that we believe depression is a system-level disorder: no single brain region or neurotransmitter is the sole driving force but instead, integrated networks of cortical and subcortical regions seem to be key (Mayberg *et al.*, 2005). This means the impact of STN-DBS on affective networks based on patients' connectivity profiles is surely not the only factor contributing to changes in depressive symptoms. Importantly, our patients had minor to moderate depressive symptoms that were partially modulated by DBS but none of them had a severe depression. Yet, this research may contribute to better understand, avoid and treat affective side effects like depressive symptoms in patients with STN-DBS.

There are several limitations that should be considered when interpreting our findings. First, there might be differences in the assessment of depressive symptoms across DBS centres, that is e.g. whether patients reported their mood state at the first or the last day of their follow-up stay when clinical interventions taken might already have improved their mood state. We do believe though that with our large sample size slight variances in the timepoint of BDI-II assessment did not systematically bias our results. Secondly, there is a variation in electrode type in the patients included in this study. This could have effects on the VTA model, e.g. by the respective consideration of constant voltage versus constant current default settings in DBS systems by Medtronic vs. Boston Scientific. To circumvent a bias of this factor, we reran analyses using the unthresholded E-field that surrounded electrodes and found the similar results. Third, we used a Parkinson-specific normative connectome for our analysis purposes, which assumes structural connectivity to be approximately the same in all patients of our sample. While this assumption might not hold true in all cases, the method has been used and

bioRxiv preprint doi: https://doi.org/10.1101/665976; this version posted June 10, 2019. The copyright holder for this preprint (which was not certified by peer review) is the author/funder. All rights reserved. No reuse allowed without permission.

validated in several recent studies with DBS context (Baldermann *et al.*, 2019; Horn *et al.*, 2017a; Neumann *et al.*, 2018). Beyond practical advantages (where patient-specific connectivity data is often not available and cannot be acquired postoperatively), normative connectomes have often been acquired on specialized MRI hardware and comprise of a high N of subjects (such in this sample of patients from the PPMI project). Thus, the use of normative connectomes has the advantage of high signal-to-noise levels and state-of-the-art data quality. Finally, we only had UPDRS-III scores ON medication (preoperative vs. ON stim) in our sample. Thus, the pre- to postoperative comparison might not reflect the full impact of STN-DBS on motor symptoms. However, since the BDI-II maps we calculated are very robustly predictive in out-of-sample data (cross-predicting between BER and QU, predicting CGN from BER/QU and predicting each patient's BDI-II improvement of the whole sample in a leave-one-out fashion), the effects of UPDRS-III improvement do not seem to have a strong impact on BDI-II either way.

In conclusion, the present results have a potential therapeutic value for the refinement of brain stimulation targets. In personalized brain stimulation, identifying proximity to fibres connecting the electrode with the left dlPFC might have a prognostic utility in predicting change in depressive symptoms under STN-DBS. Prospectively, connectivity maps as the one presented here as well as isolated fibertracts can be used in surgical planning to optimize positioning of DBS leads in PD patients. Furthermore, with the use of directional leads, the electrical field could be guided away from fibertracts anteromedial to the left STN, the stimulation of which was associated with depressive symptoms in our study. Importantly, this study specifically shows that the STN connectivity profiles might have to be treated differently for the right and left hemisphere. However, more work is needed to validate this presumption based on patient-specific connectivity. Altogether, our findings lead to a better understanding of how negative mood effects may originate following STN-DBS and pave the way toward personalized brain stimulation in which individual connectivity profiles and symptom constellations determine optimal DBS targets.

bioRxiv preprint doi: https://doi.org/10.1101/665976; this version posted June 10, 2019. The copyright holder for this preprint (which was not certified by peer review) is the author/funder. All rights reserved. No reuse allowed without permission.

Acknowledgements

We thank Alexandra Horn for her valuable contribution in the data analysis.

Data used in the preparation of this article were obtained from the Parkinson's Progression Markers Initiative (PPMI) database (www.ppmi-info.org/data). For up-to-date information on the study, visit www.ppmi-info.org. PPMI - a public-private partnership - is funded by the Michael J. Fox Foundation for Parkinson's Research and funding partners, see www.ppmi-info.org/fundingpartners.

Funding sources for the study

This study was supported by the Deutsche Forschungsgemeinschaft (DFG grant SPP2041, "Clinical connectomics: a network approach to deep brainstimulation" to A.A.K. as well as Emmy Noether Grant 410169619 to A.H.).

Competing Interests

A.A.K. has received honoraria as speaker for Boston Scientific, Abbott and Medtronic, all maker for DBS devices, which is not related to the current work. A.H. has received one-time speaker honorarium by Medtronic not related to the current work. J.N.P.S. has received a travel grant by Boston Scientific not related to the current work. V.V.V. has received honoraria as speaker and/or contributions to advisory board meetings for Boston Scientific, Abbott and Medtronic, all maker for DBS devices, which is not related to the current work.

bioRxiv preprint doi: https://doi.org/10.1101/665976; this version posted June 10, 2019. The copyright holder for this preprint (which was not certified by peer review) is the author/funder. All rights reserved. No reuse allowed without permission.

References

Accolla, E. A., Dukart, J., Helms, G., Weiskopf, N., Kherif, F., Lutti, A., … Draganski, B. (2014). Brain tissue properties differentiate between motor and limbic basal ganglia circuits. *Human Brain Mapping*, *35*(10), 5083–5092. https://doi.org/10.1002/hbm.22533

Accolla, E. A., Herrojo Ruiz, M., Horn, A., Schneider, G.-H., Schmitz-Hübsch, T., Draganski, B., & Kühn, A. A. (2016). Brain networks modulated by subthalamic nucleus deep brain stimulation. *Brain*, *139*(Pt 9), 2503–2515.

Accolla, E. A., Horn, A., Herrojo-Ruiz, M., Neumann, W.-J., & Kühn, A. A. (2017). Reply: Oscillatory coupling of the subthalamic nucleus in obsessive compulsive disorder. *Brain*, *140*(9), e57–e57. Retrieved from http://dx.doi.org/10.1093/brain/awx165

Alexander, G. E., & Crutcher, M. D. (1990). Functional architecture of basal ganglia circuits: neural substrates of parallel processing. *TINS*, *13*(7), 266–271.

Amunts, K., Lepage, C., Borgeat, L., Mohlberg, H., Dickscheid, T., Rousseau, M.-É., … Evans, A. C. (2013). BigBrain: An Ultrahigh-Resolution 3D Human Brain Model. *Science*, *340*(6139), 1472 LP – 1475. https://doi.org/10.1126/science.1235381

Appleby, B. S., Duggan, P. S., Regenberg, A., & Rabins, P. V. (2007). Psychiatric and neuropsychiatric adverse events associated with deep brain stimulation: A meta-analysis of ten years' experience. *Movement Disorders*, *22*(12), 1722–1728. https://doi.org/10.1002/mds.21551

Aron, A. R., Herz, D. M., Brown, P., Forstmann, B. U., & Zaghloul, K. (2016). Frontosubthalamic Circuits for Control of Action and Cognition. *The Journal of Neuroscience*, *36*(45), 11489–11495. https://doi.org/10.1523/JNEUROSCI.2348-16.2016

Ashburner, J., & Friston, K. J. (2005). Unified segmentation. *NeuroImage*, *26*(3), 839–851. https://doi.org/10.1016/J.NEUROIMAGE.2005.02.018

Avants, B. B., Epstein, C. L., Grossman, M., & Gee, J. C. (2008). Symmetric diffeomorphic image registration with cross-correlation: Evaluating automated labeling of elderly and neurodegenerative brain. *Medical Image Analysis*, *12*(1), 26–41. https://doi.org/10.1016/j.media.2007.06.004

Baldermann, J. C., Melzer, C., Zapf, A., Kohl, S., Timmermann, L., Tittgemeyer, M., … Kuhn, J. (2019). Connectivity Profile Predictive of Effective Deep Brain Stimulation in Obsessive-Compulsive Disorder. *Biological Psychiatry*. https://doi.org/10.1016/J.BIOPSYCH.2018.12.019

Beck, A. T., Steer, R. A., & Brown, G. k. (1996). *Manual for the Beck Depression Inventory-II*. San Antonio, TX: Psychological Corporation.

bioRxiv preprint doi: https://doi.org/10.1101/665976; this version posted June 10, 2019. The copyright holder for this preprint (which was not certified by peer review) is the author/funder. All rights reserved. No reuse allowed without permission.

Bejjani, B.-P., Damier, P., Arnulf, I., Thivard, L., Bonnet, A.-M., Dormont, D., … Agid, Y. (1999). Transient Acute Depression Induced by High-Frequency Deep-Brain Stimulation. *New England Journal of Medicine*, *340*(19), 1476–1480. https://doi.org/10.1056/nejm199905133401905

Belujon, P., & Grace, A. A. (2017). Dopamine system dysregulation in major depressive disorders. *International Journal of Neuropsychopharmacology*, *20*(12), 1036–1046. https://doi.org/10.1093/ijnp/pyx056

Campbell, M.C., Karimi, M., Weaver, P. M., Wu, J., Perantie, D. C., Golchin, N. A., … Hershey, T. (2008). Neural correlates of STN DBS-induced cognitive variability in Parkinson disease. *Neuropsychologia*, *46*(13), 3162–3169. https://doi.org/10.1016/J.NEUROPSYCHOLOGIA.2008.07.012

Campbell, Meghan C, Black, K. J., Weaver, P. M., Lugar, H. M., Videen, T. O., Tabbal, S. D., … Hershey, T. (2012). Mood response to deep brain stimulation of the subthalamic nucleus in Parkinson's disease. *The Journal of Neuropsychiatry and Clinical Neurosciences*, *24*(1), 28–36. https://doi.org/10.1176/appi.neuropsych.11030060

Castrioto, A., Lhommée, E., Moro, E., & Krack, P. (2014). Mood and behavioural effects of subthalamic stimulation in Parkinson's disease. *The Lancet. Neurology*, *13*(3), 287–305. https://doi.org/10.1016/S1474-4422(13)70294-1

Cavanagh, J. F., Wiecki, T. V, Cohen, M. X., Figueroa, C. M., Samanta, J., Sherman, S. J., & Frank, M. J. (2011). Subthalamic nucleus stimulation reverses mediofrontal influence over decision threshold. *Nature Neuroscience*, *14*(11), 1462–1467. https://doi.org/10.1038/nn.2925

Chang, C.-C., Yu, S.-C., McQuoid, D. R., Messer, D. F., Taylor, W. D., Singh, K., … Payne, M. E. (2011). Reduction of dorsolateral prefrontal cortex gray matter in late-life depression. *Psychiatry Research*, *193*(1), 1–6. https://doi.org/10.1016/j.pscychresns.2011.01.003

Chaudhuri, K. R., & Schapira, A. H. V. (2009). Non-motor symptoms of Parkinson's disease: dopaminergic pathophysiology and treatment. *The Lancet Neurology*, *8*(5), 464–474. https://doi.org/10.1016/S1474-4422(09)70068-7

Chopra, A., Tye, S. J., Lee, K. H., Matsumoto, J., Klassen, B., Adams, A. C., … Frye, M. A. (2011). Voltage-Dependent Mania After Subthalamic Nucleus Deep Brain Stimulation in Parkinson's Disease: A Case Report. *Biological Psychiatry*, *70*(2), e5–e7. https://doi.org/10.1016/j.biopsych.2010.12.035

Dafsari, H S, Ray-Chaudhuri, K., Mahlstedt, P., Sachse, L., Steffen, J. K., Petry-Schmelzer, J.

bioRxiv preprint doi: https://doi.org/10.1101/665976; this version posted June 10, 2019. The copyright holder for this preprint (which was not certified by peer review) is the author/funder. All rights reserved. No reuse allowed without permission.

N., … Timmermann, L. (2019). Beneficial effects of bilateral subthalamic stimulation on alexithymia in Parkinson's disease. *European Journal of Neurology*, *26*(2), 222-e17. https://doi.org/10.1111/ene.13773

Dafsari, Haidar S., Silverdale, M., Strack, M., Rizos, A., Ashkan, K., Mahlstedt, P., … Timmermann, L. (2018). Nonmotor symptoms evolution during 24 months of bilateral subthalamic stimulation in Parkinson's disease. *Movement Disorders*, *33*(3), 421–430. https://doi.org/10.1002/mds.27283

Dafsari, Haidar Salimi, Petry-Schmelzer, J. N., Ray-Chaudhuri, K., Ashkan, K., Weis, L., Dembek, T. A., … Timmermann, L. (2018a). Non-motor outcomes of subthalamic stimulation in Parkinson's disease depend on location of active contacts. *Brain Stimulation*, *11*(4), 904–912. https://doi.org/10.1016/j.brs.2018.03.009

Dafsari, Haidar Salimi, Petry-Schmelzer, J. N., Ray-Chaudhuri, K., Ashkan, K., Weis, L., Dembek, T. A., … Timmermann, L. (2018b). Non-motor outcomes of subthalamic stimulation in Parkinson's disease depend on location of active contacts. *Brain Stimulation*, *11*(4), 904–912. https://doi.org/10.1016/J.BRS.2018.03.009

Daniele, A., Albanese, A., Contarino, M. F., Zinzi, P., Barbier, A., Gasparini, F., … Scerrati, M. (2003). Cognitive and behavioural effects of chronic stimulation of the subthalamic nucleus in patients with Parkinson's disease. *J Neurol.Neurosurg.Psychiatry*, *74*(2), 175–182. https://doi.org/10.1136/jnnp.74.2.175

Deuschl, G., Schade-Brittinger, C., Krack, P., Volkmann, J., Schäfer, H., Bötzel, K., … Voges, J. (2006). A Randomized Trial of Deep-Brain Stimulation for Parkinson's Disease. *New England Journal of Medicine*, *355*(9), 896–908. https://doi.org/10.1056/NEJMoa060281

Dunlop, B. W., & Nemeroff, C. B. (2007). The Role of Dopamine in the Pathophysiology of Depression. *Archives of General Psychiatry*, *64*, 327–337. https://doi.org/10.1001/archpsyc.64.3.327

Edlow, B. L., Takahashi, E., Wu, O., Benner, T., Dai, G., Bu, L., … Folkerth, R. D. (2012). Neuroanatomic Connectivity of the Human Ascending Arousal System Critical to Consciousness and Its Disorders. *Journal of Neuropathology & Experimental Neurology*, *71*(6), 531–546. https://doi.org/10.1097/NEN.0b013e3182588293

Egorova, N., Brodtmann, A., Veldsman, M., Werden, E., Shirbin, C., & Cumming, T. (2017). Lower cognitive control network connectivity in stroke participants with depressive features. *Translational Psychiatry*, *7*(11), 1–7. https://doi.org/10.1038/s41398-017-0038-x

bioRxiv preprint doi: https://doi.org/10.1101/665976; this version posted June 10, 2019. The copyright holder for this preprint (which was not certified by peer review) is the author/funder. All rights reserved. No reuse allowed without permission.

Eisenstein, S. A., Koller, J. M., Black, K. D., Campbell, M. C., Lugar, H. M., Ushe, M., … Black, K. J. (2014). Functional anatomy of subthalamic nucleus stimulation in Parkinson disease. *Annals of Neurology*, *76*(2), 279–295. https://doi.org/10.1002/ana.24204

Eitan, R., Shamir, R., Linetsky, E., Rosenbluh, O., Moshel, S., Ben-Hur, T., … Israel, Z. (2013). Asymmetric right/left encoding of emotions in the human subthalamic nucleus . *Frontiers in Systems Neuroscience* . Retrieved from https://www.frontiersin.org/article/10.3389/fnsys.2013.00069

Emre, M., Aarsland, D., Brown, R., Burn, D. J., Duyckaerts, C., Mizuno, Y., … Dubois, B. (2007). Clinical diagnostic criteria for dementia associated with Parkinson's disease. *Movement Disorders*, *22*(12), 1689–1707. https://doi.org/10.1002/mds.21507

Ewert, S., Horn, A., Finkel, F., Li, N., Kühn, A. A., & Herrington, T. M. (2019). Optimization and comparative evaluation of nonlinear deformation algorithms for atlas-based segmentation of DBS target nuclei. *NeuroImage*, *184*, 586–598. https://doi.org/10.1016/J.NEUROIMAGE.2018.09.061

Ewert, S., Plettig, P., Li, N., Chakravarty, M. M., Collins, D. L., Herrington, T. M., … Horn, A. (2017). Toward defining deep brain stimulation targets in MNI space: A subcortical atlas based on multimodal MRI, histology and structural connectivity. *NeuroImage*. https://doi.org/https://doi.org/10.1016/j.neuroimage.2017.05.015

Fasano, A., Daniele, A., & Albanese, A. (2012). Treatment of motor and non-motor features of Parkinson's disease with deep brain stimulation. *The Lancet Neurology*, *11*(5), 429–442. https://doi.org/10.1016/S1474-4422(12)70049-2

Fedorof, JP Starkstein, SE Forrester, AW Geisler, FH Jorge, R., & Arndt, SV Robinson, R. (1992). Depression in patients with acute traumatic brain injury. *American Journal of Psychiatry*, *149*(7), 918–923. https://doi.org/10.1176/ajp.149.7.918

Follett, K. A., Weaver, F. M., Stern, M., Hur, K., Harris, C. L., Luo, P., … Reda, D. J. (2010). Pallidal versus Subthalamic Deep-Brain Stimulation for Parkinson's Disease. *New England Journal of Medicine*, *362*(22), 2077–2091. https://doi.org/10.1056/NEJMoa0907083

Forstmann, B. U., de Hollander, G., van Maanen, L., Alkemade, A., & Keuken, M. C. (2016). Towards a mechanistic understanding of the human subcortex. *Nature Reviews Neuroscience*, *18*, 57. Retrieved from https://doi.org/10.1038/nrn.2016.163

Fox, M. D., Buckner, R. L., White, M. P., Greicius, M. D., & Pascual-Leone, A. (2012). Efficacy of transcranial magnetic stimulation targets for depression is related to intrinsic functional connectivity with the subgenual cingulate. *Biological Psychiatry*, *72*(7), 595–

bioRxiv preprint doi: https://doi.org/10.1101/665976; this version posted June 10, 2019. The copyright holder for this preprint (which was not certified by peer review) is the author/funder. All rights reserved. No reuse allowed without permission.

603. https://doi.org/10.1016/j.biopsych.2012.04.028

Fox, M. D., Liu, H., & Pascual-Leone, A. (2013). Identification of reproducible individualized targets for treatment of depression with TMS based on intrinsic connectivity. *NeuroImage*, *66*, 151–160. https://doi.org/10.1016/J.NEUROIMAGE.2012.10.082

Frank, M. J., Samanta, J., Moustafa, A. a, & Sherman, S. J. (2007). Hold your horses: impulsivity, deep brain stimulation, and medication in parkinsonism. *Science (New York, N.Y.)*, *318*(5854), 1309–1312. https://doi.org/10.1126/science.1146157

Funkiewiez, A., Ardouin, C., Cools, R., Krack, P., Fraix, V., Batir, A., … Pollak, P. (2006). Effects of levodopa and subthalamic nucleus stimulation on cognitive and affective functioning in Parkinson's disease. *Movement Disorders*, *21*(10), 1656–1662. https://doi.org/10.1002/mds.21029

Funkiewiez, A., Ardouin, C., Krack, P., Fraix, V., Van Blercom, N., Xie, J., … Pollak, P. (2003). Acute psychotropic effects of bilateral subthalamic nucleus stimulation and levodopa in Parkinson's disease. *Movement Disorders*, *18*(5), 524–530. https://doi.org/10.1002/mds.10441

Grajny, K., Pyata, H., Spiegel, K., Lacey, E. H., Xing, S., Brophy, C., & Turkeltaub, P. E. (2016). Depression Symptoms in Chronic Left Hemisphere Stroke Are Related to Dorsolateral Prefrontal Cortex Damage. *The Journal of Neuropsychiatry and Clinical Neurosciences*, *28*(4), 292–298. https://doi.org/10.1176/appi.neuropsych.16010004

Grimm, S., Beck, J., Schuepbach, D., Hell, D., Boeker, H., Boesiger, P., … Northoff, G. (2007). Imbalance between Left and Right Dorsolateral Prefrontal Cortex in Major Depression Is Linked to Negative Emotional Judgment: An fMRI Study in Severe Major Depressive Disorder. *Biological Psychiatry*, *63*(4), 369–376. https://doi.org/10.1016/j.biopsych.2007.05.033

Hajós, M., Richards, C. D., Székely, A. D., & Sharp, T. (1998). An electrophysiological and neuroanatomical study of the medial prefrontal cortical projection to the midbrain raphe nuclei in the rat. *Neuroscience*, *87*(1), 95–108. https://doi.org/https://doi.org/10.1016/S0306-4522(98)00157-2

Hama, S., Yamashita, H., Shigenobu, M., Watanabe, A., Kurisu, K., Yamawaki, S., & Kitaoka, T. (2007). Post-stroke affective or apathetic depression and lesion location: left frontal lobe and bilateral basal ganglia. *European Archives of Psychiatry and Clinical Neuroscience*, *257*(3), 149–152. https://doi.org/10.1007/s00406-006-0698-7

Hamilton, J. P., Ph, D., Lemus, M. G., Johnson, R. F., Gotlib, I. H., & Ph, D. (2012).

bioRxiv preprint doi: https://doi.org/10.1101/665976; this version posted June 10, 2019. The copyright holder for this preprint (which was not certified by peer review) is the author/funder. All rights reserved. No reuse allowed without permission.

Functional neroimaging of major depressive disorder: a meta-analysis and new intergration of baseline activation and neural response data. *American Journal of Psychiatry*, *169*(7), 693–703.

Hartung, H., Tan, S. K. H., Steinbusch, H. M. W., Temel, Y., & Sharp, T. (2011). High-frequency stimulation of the subthalamic nucleus inhibits the firing of juxtacellular labelled 5-HT-containing neurones. *Neuroscience*, *186*, 135–145. https://doi.org/https://doi.org/10.1016/j.neuroscience.2011.04.004

Haynes, W. I. A., & Haber, S. N. (2013). The organization of prefrontal-subthalamic inputs in primates provides an anatomical substrate for both functional specificity and integration: implications for basl ganglia models and deep brain stimulation. *J Neuroscience*, *33*(11), 4804–4814.

Hellerbach, A., Dembek, T. A., Hoevels, M., Holz, J. A., Gierich, A., Luyken, K., … Treuer, H. (2018). DiODe: Directional Orientation Detection of Segmented Deep Brain Stimulation Leads: A Sequential Algorithm Based on CT Imaging. *Stereotactic and Functional Neurosurgery*, *96*(5), 335–341. https://doi.org/10.1159/000494738

Herz, D. M., Zavala, B. A., Bogacz, R., & Brown, P. (2016). Neural Correlates of Decision Thresholds in the Human Subthalamic Nucleus. *Current Biology*, *26*(7), 916–920. https://doi.org/10.1016/j.cub.2016.01.051

Horn, A., & Kühn, A. A. (2015). Lead-DBS: A toolbox for deep brain stimulation electrode localizations and visualizations. *NeuroImage*, *107*, 127–135. https://doi.org/10.1016/j.neuroimage.2014.12.002

Horn, A., Kühn, A. A., Merkl, A., Shih, L., Alterman, R., & Fox, M. (2017). Probabilistic conversion of neurosurgical DBS electrode coordinates into MNI space. *NeuroImage*, *150*(Supplement C), 395–404. https://doi.org/https://doi.org/10.1016/j.neuroimage.2017.02.004

Horn, A., Li, N., Dembek, T. A., Kappel, A., Boulay, C., Ewert, S., … Kühn, A. A. (2019). Lead-DBS v2: Towards a comprehensive pipeline for deep brain stimulation imaging. *NeuroImage*, *184*, 293–316. https://doi.org/10.1016/J.NEUROIMAGE.2018.08.068

Horn, A., Ostwald, D., Reisert, M., & Blankenburg, F. (2014). The structural-functional connectome and the default mode network of the human brain. *NeuroImage*, *102*(P1), 142–151. https://doi.org/10.1016/j.neuroimage.2013.09.069

Horn, A., Reich, M., Vorwerk, J., Li, N., Wenzel, G., Fang, Q., … Fox, M. D. (2017). Connectivity Predicts deep brain stimulation outcome in Parkinson disease. *Annals of Neurology*, *82*(1), 67–78. https://doi.org/10.1002/ana.24974

bioRxiv preprint doi: https://doi.org/10.1101/665976; this version posted June 10, 2019. The copyright holder for this preprint (which was not certified by peer review) is the author/funder. All rights reserved. No reuse allowed without permission.

Horn, A., Wenzel, G., Irmen, F., Huebl, J., Li, N., Neumann, W.-J., … Kuehn, A. A. (2019). Modulating the human functional connectome using deep brain stimulation. *BioRxiv*, 537712. https://doi.org/10.1101/537712

Husch, A., V. Petersen, M., Gemmar, P., Goncalves, J., & Hertel, F. (2018). PaCER - A fully automated method for electrode trajectory and contact reconstruction in deep brain stimulation. *NeuroImage: Clinical*, *17*, 80–89. https://doi.org/10.1016/J.NICL.2017.10.004

Hwang, J. W., Egorova, N., Yang, X. Q., Zhang, W. Y., Chen, J., Yang, X. Y., … Kong, J. (2015). Subthreshold depression is associated with impaired resting-state functional connectivity of the cognitive control network. *Translational Psychiatry*, *5*, e683. Retrieved from https://doi.org/10.1038/tp.2015.174

Ikuta, T., Matsuo, K., Harada, K., Nakashima, M., Hobara, T., Higuchi, N., … Watanabe, Y. (2017). Disconnectivity between Dorsal Raphe Nucleus and Posterior Cingulate Cortex in Later Life Depression . *Frontiers in Aging Neuroscience* . Retrieved from https://www.frontiersin.org/article/10.3389/fnagi.2017.00236

Irmen, F., Horn, A., Meder, D., Neumann, W.-J., Plettig, P., Schneider, G.-H., … Kühn, A. A. (2019). Sensorimotor subthalamic stimulation restores risk-reward trade-off in Parkinson's disease. *Movement Disorders*, *34*(3), 366–376. https://doi.org/10.1002/mds.27576

Irmen, F., Huebl, J., Schroll, H., Brücke, C., Schneider, G.-H., Hamker, F. H., & Kühn, A. A. (2017). Subthalamic nucleus stimulation impairs emotional conflict adaptation in Parkinson's disease. *Social Cognitive and Affective Neuroscience*, *12*(10), 1594–1604. https://doi.org/10.1093/scan/nsx090

Jorge, R. E., Robinson, R. G., Moser, D., Tateno, A., Crespo-Facorro, B., & Arndt, S. (2004). Major Depression Following Traumatic Brain Injury. *Archives of General Psychiatry*, *61*(1), 42–50. https://doi.org/10.1001/archpsyc.61.1.42

Kaiser, R. H., Andrews-Hanna, J. R., Wager, T. D., & Pizzagalli, D. A. (2015). Large-Scale Network Dysfunction in Major Depressive Disorder: A Meta-analysis of Resting-State Functional ConnectivityMeta-analysis of Network Dysfunction in DepressionMeta-analysis of Network Dysfunction in Depression. *JAMA Psychiatry*, *72*(6), 603–611. https://doi.org/10.1001/jamapsychiatry.2015.0071

Koenigs, M., & Grafman, J. (2009). The functional neuroanatomy of depression: Distinct roles for ventromedial and dorsolateral prefrontal cortex. *Behav Brain Res*, *201*(2), 239–243. https://doi.org/10.1016/j.bbr.2009.03.004.The

bioRxiv preprint doi: https://doi.org/10.1101/665976; this version posted June 10, 2019. The copyright holder for this preprint (which was not certified by peer review) is the author/funder. All rights reserved. No reuse allowed without permission.

Koenigs, M., Huey, E. D., Calamia, M., Raymont, V., Tranel, D., & Grafman, J. (2008). Distinct Regions of Prefrontal Cortex Mediate Resistance and Vulnerability to Depression. *The Journal of Neuroscience*, *28*(47), 12341 LP – 12348. https://doi.org/10.1523/JNEUROSCI.2324-08.2008

Krack, P., Hariz, M. I., Baunez, C., Guridi, J., & Obeso, J. A. (2010). Deep brain stimulation: From neurology to psychiatry? *Trends in Neurosciences*, *33*(10), 474–484. https://doi.org/10.1016/j.tins.2010.07.002

Kurtis, M. M., Rajah, T., Delgado, L. F., & Dafsari, H. S. (2017). The effect of deep brain stimulation on the non-motor symptoms of Parkinson's disease: a critical review of the current evidence. *Npj Parkinson's Disease*, *3*(1), 1–12. https://doi.org/10.1038/npjparkd.2016.24

Leung, A., Metzger-Smith, V., He, Y., Cordero, J., Ehlert, B., Song, D., … Lee, R. (2018). Left Dorsolateral Prefrontal Cortex rTMS in Alleviating MTBI Related Headaches and Depressive Symptoms. *Neuromodulation: Technology at the Neural Interface*, *21*(4), 390–401. https://doi.org/10.1111/ner.12615

Lévesque, J., Eugène, F., Joanette, Y., Paquette, V., Mensour, B., Beaudoin, G., … Beauregard, M. (2003). Neural circuitry underlying voluntary suppression of sadness. *Biological Psychiatry*, *53*(6), 502–510. https://doi.org/10.1016/S0006-3223(02)01817-6

Li, N., Baldermann, J. C., Kibleur, A., Treu, S., Elias, G. J. B., Boutet, A., … Horn, A. (2019). Toward a unified connectomic target for deep brain stimulation in obsessive-compulsive disorder. *BioRxiv*, 608786. https://doi.org/10.1101/608786

Lozano, A. M., & Lipsman, N. (2013). Probing and Regulating Dysfunctional Circuits Using Deep Brain Stimulation. *Neuron*, *77*(3), 406–424. https://doi.org/10.1016/J.NEURON.2013.01.020

Mallet, L., Schupbach, M., N'Diaye, K., Remy, P., Bardinet, E., Czernecki, V., … Yelnik, J. (2007). Stimulation of subterritories of the subthalamic nucleus reveals its role in the integration of the emotional and motor aspects of behavior. *Proceedings of the National Academy of Sciences*, *104*(25), 10661–10666. https://doi.org/10.1073/pnas.0610849104

Marek, K., Jennings, D., Lasch, S., Siderowf, A., Tanner, C., Simuni, T., … Taylor, P. (2011). The Parkinson Progression Marker Initiative (PPMI). *Progress in Neurobiology*, *95*(4), 629–635. https://doi.org/10.1016/J.PNEUROBIO.2011.09.005

Mayberg, H., Lozano, A. M., Voon, V., McNeely, H. E., Seminowicz, D., Hamani, C., … Kennedy, S. H. (2005). Deep brain stimulation for treatment-resistant depression. *Neuron*, *45*(March 3), 651–660.

bioRxiv preprint doi: https://doi.org/10.1101/665976; this version posted June 10, 2019. The copyright holder for this preprint (which was not certified by peer review) is the author/funder. All rights reserved. No reuse allowed without permission.

Michelsen, K. A., Prickaerts, J., & Steinbusch, H. W. M. (2008). The dorsal raphe nucleus and serotonin: implications for neuroplasticity linked to major depression and Alzheimer's disease. *Progress in Brain Research*, *172*, 233–264. https://doi.org/10.1016/S0079-6123(08)00912-6

Michelsen, K. A., Schmitz, C., & Steinbusch, H. W. M. (2007). The dorsal raphe nucleus—From silver stainings to a role in depression. *Brain Research Reviews*, *55*(2), 329–342. https://doi.org/https://doi.org/10.1016/j.brainresrev.2007.01.002

Mosley, P. E., Smith, D., Coyne, T., Silburn, P., Breakspear, M., & Perry, A. (2018). The site of stimulation moderates neuropsychiatric symptoms after subthalamic deep brain stimulation for Parkinson's disease. *NeuroImage: Clinical*, *18*(March), 996–1006. https://doi.org/10.1016/j.nicl.2018.03.009

Neumann, W.-J., Schroll, H., de Almeida Marcelino, A. L., Horn, A., Ewert, S., Irmen, F., … Kühn, A. A. (2018). Functional segregation of basal ganglia pathways in Parkinson's disease. *Brain*, *141*(9), 2655–2669. https://doi.org/10.1093/brain/awy206

Ochsner, K. N., Ray, R. D., Cooper, J. C., Robertson, E. R., Chopra, S., Gabrieli, J. D. E., & Gross, J. J. (2004). For better or for worse: neural systems supporting the cognitive down- and up-regulation of negative emotion. *NeuroImage*, *23*(2), 483–499. https://doi.org/10.1016/J.NEUROIMAGE.2004.06.030

Okun, M. S., Fernandez, H. H., Wu, S. S., Kirsch-Darrow, L., Bowers, D., Bova, F., … Foote, K. D. (2009). Cognition and mood in Parkinson's disease in subthalamic nucleus versus globus pallidus interna deep brain stimulation: The COMPARE Trial. *Annals of Neurology*, *65*(5), 586–595. https://doi.org/10.1002/ana.21596

Pan, J., Zhan, L., Hu, C., Yang, J., Wang, C., Gu, L., … Wu, X. (2018). Emotion Regulation and Complex Brain Networks: Association Between Expressive Suppression and Efficiency in the Fronto-Parietal Network and Default-Mode Network. *Frontiers in Human Neuroscience*, *12*(March), 1–12. https://doi.org/10.3389/fnhum.2018.00070

Pascual-Leone, A., Rubio, B., Pallardó, F., & Catalá, M. D. (1996). Rapid-rate transcranial magnetic stimulation of left dorsolateral prefrontal cortex in drug-resistant depression. *Lancet*, *348*(9022), 233–237. https://doi.org/10.1016/S0140-6736(96)01219-6

Péron, J., Biseul, I., Leray, E., Vicente, S., Le Jeune, F., Drapier, S., … Vérin, M. (2010). Subthalamic nucleus stimulation affects fear and sadness recognition in Parkinson's disease. *Neuropsychology*, *24*(1), 1–8. https://doi.org/10.1037/a0017433

Péron, J., Frühholz, S., Ceravolo, L., & Grandjean, D. (2015). Structural and functional connectivity of the subthalamic nucleus during vocal emotion decoding. *Social Cognitive*

bioRxiv preprint doi: https://doi.org/10.1101/665976; this version posted June 10, 2019. The copyright holder for this preprint (which was not certified by peer review) is the author/funder. All rights reserved. No reuse allowed without permission.

and Affective Neuroscience, *11*(2), 349–356. https://doi.org/10.1093/scan/nsv118

Péron, J., Frühholz, S., Vérin, M., & Grandjean, D. (2013). Subthalamic nucleus: A key structure for emotional component synchronization in humans. *Neuroscience and Biobehavioral Reviews*, *37*(3), 358–373. https://doi.org/10.1016/j.neubiorev.2013.01.001

Peyron, C., Petit, J.-M., Rampon, C., Jouvet, M., & Luppi, P.-H. (1997). Forebrain afferents to the rat dorsal raphe nucleus demonstrated by retrograde and anterograde tracing methods. *Neuroscience*, *82*(2), 443–468. https://doi.org/https://doi.org/10.1016/S0306-4522(97)00268-6

Phan, K. L., Fitzgerald, D. A., Nathan, P. J., Moore, G. J., Uhde, T. W., & Tancer, M. E. (2005). Neural substrates for voluntary suppression of negative affect: A functional magnetic resonance imaging study. *Biological Psychiatry*, *57*(3), 210–219. https://doi.org/10.1016/j.biopsych.2004.10.030

Philip, N. S., Barredo, J., Aiken, E., & Carpenter, L. L. (2018). Neuroimaging Mechanisms of Therapeutic Transcranial Magnetic Stimulation for Major Depressive Disorder. *Biological Psychiatry: Cognitive Neuroscience and Neuroimaging*, *3*(3), 211–222. https://doi.org/10.1016/J.BPSC.2017.10.007

Politis, M., Wu, K., Loane, C., Turkheimer, F. E., Molloy, S., Brooks, D. J., & Piccini, P. (2010). Depressive symptoms in PD correlate with higher 5-HTT binding in raphe and limbic structures. *Neurology*, *75*(21), 1920 LP – 1927. https://doi.org/10.1212/WNL.0b013e3181feb2ab

Qamhawi, Z., Towey, D., Shah, B., Pagano, G., Seibyl, J., Marek, K., … Pavese, N. (2015). Clinical correlates of raphe serotonergic dysfunction in early Parkinson's disease. *Brain*, *138*(10), 2964–2973. https://doi.org/10.1093/brain/awv215

Rodriguez-Oroz, M. C., López-Azcárate, J., Garcia-Garcia, D., Alegre, M., Toledo, J., Valencia, M., … Obeso, J. A. (2011). Involvement of the subthalamic nucleus in impulse control disorders associated with Parkinson's disease. *Brain*, *134*(1), 36–49. https://doi.org/10.1093/brain/awq301

Romito, L. M., Raja, M., Daniele, A., Contarino, M. F., Bentivoglio, A. R., Barbier, A., … Albanese, A. (2002). Transient mania with hypersexuality after surgery for high frequency stimulation of the subthalamic nucleus in Parkinson's disease. *Movement Disorders*, *17*(6), 1371–1374. https://doi.org/10.1002/mds.10265

Sheline, Y. I., Price, J. L., Yan, Z., & Mintun, M. A. (2010). Resting-state functional MRI in depression unmasks increased connectivity between networks via the dorsal nexus. *Proceedings of the National Academy of Sciences of the United States of America*,

bioRxiv preprint doi: https://doi.org/10.1101/665976; this version posted June 10, 2019. The copyright holder for this preprint (which was not certified by peer review) is the author/funder. All rights reserved. No reuse allowed without permission.

107(24), 11020–11025. https://doi.org/10.1073/pnas.1000446107

Shi, Y., Yang, D., Zeng, Y., & Wu, W. (2017). Risk Factors for Post-stroke Depression: A Meta-analysis. *Frontiers in Aging Neuroscience*, *9*, 218. https://doi.org/10.3389/fnagi.2017.00218

Sieger, T., Serranová, T., Růžička, F., Vostatek, P., Wild, J., Šťastná, D., … Jech, R. (2015). Distinct populations of neurons respond to emotional valence and arousal in the human subthalamic nucleus. *Proceedings of the National Academy of Sciences*, *112*(10), 3116–3121. https://doi.org/10.1073/pnas.1410709112

Sitz, A., Hoevels, M., Hellerbach, A., Gierich, A., Luyken, K., Dembek, T. A., … Treuer, H. (2017). Determining the orientation angle of directional leads for deep brain stimulation using computed tomography and digital x-ray imaging: A phantom study. *Medical Physics*, *44*(9), 4463–4473. https://doi.org/10.1002/mp.12424

Tan, S. K. H., Janssen, M. L. F., Jahanshahi, A., Chouliaras, L., Visser-Vandewalle, V., Lim, L. W., … Temel, Y. (2011). High frequency stimulation of the subthalamic nucleus increases c-fos immunoreactivity in the dorsal raphe nucleus and afferent brain regions. *Journal of Psychiatric Research*, *45*(10), 1307–1315. https://doi.org/https://doi.org/10.1016/j.jpsychires.2011.04.011

Temel, Y., Boothman, L. J., Blokland, A., Magill, P. J., Steinbusch, H. W. M., Visser-Vandewalle, V., & Sharp, T. (2007). Inhibition of 5-HT neuron activity and induction of depressive-like behavior by high-frequency stimulation of the subthalamic nucleus. *Proceedings of the National Academy of Sciences of the United States of America*, *104*(43), 17087–17092. https://doi.org/10.1073/pnas.0704144104

Temel, Y., Kessels, A., Tan, S., Topdag, A., Boon, P., & Visser-Vandewalle, V. (2006). Behavioural changes after bilateral subthalamic stimulation in advanced Parkinson disease: A systematic review. *Parkinsonism & Related Disorders*, *12*(5), 265–272. https://doi.org/10.1016/J.PARKRELDIS.2006.01.004

Thobois, S., Ardouin, C., Lhommée, E., Klinger, H., Lagrange, C., Xie, J., … Krack, P. (2010). Non-motor dopamine withdrawal syndrome after surgery for Parkinson's disease: predictors and underlying mesolimbic denervation. *Brain*, *133*(4), 1111–1127. Retrieved from http://dx.doi.org/10.1093/brain/awq032

Thomas, A. J., Perry, R., Kalaria, R. N., Oakley, A., McMeekin, W., & O'Brien, J. T. (2003). Neuropathological evidence for ischemia in the white matter of the dorsolateral prefrontal cortex in late-life depression. *International Journal of Geriatric Psychiatry*, *18*(1), 7–13. https://doi.org/10.1002/gps.720

bioRxiv preprint doi: https://doi.org/10.1101/665976; this version posted June 10, 2019. The copyright holder for this preprint (which was not certified by peer review) is the author/funder. All rights reserved. No reuse allowed without permission.

Varga, V., Kocsis, B., & Sharp, T. (2003). Electrophysiological evidence for convergence of inputs from the medial prefrontal cortex and lateral habenula on single neurons in the dorsal raphe nucleus. *European Journal of Neuroscience*, *17*(2), 280–286. https://doi.org/10.1046/j.1460-9568.2003.02465.x

Varga, V., Székely, A. D., Csillag, A., Sharp, T., & Hajós, M. (2001). Evidence for a role of GABA interneurones in the cortical modulation of midbrain 5-hydroxytryptamine neurones. *Neuroscience*, *106*(4), 783–792. https://doi.org/https://doi.org/10.1016/S0306-4522(01)00294-9

Volkmann, J., Daniels, C., & Witt, K. (2010). Neuropsychiatric effects of subthalamic neurostimulation in Parkinson disease. *Nature Reviews Neurology*, 1–12. https://doi.org/10.1038/nrneurol.2010.111

Voon, V., Krack, P., Lang, A. E., Lozano, A. M., Dujardin, K., Schüpbach, M., … Moro, E. (2008). A multicentre study on suicide outcomes following subthalamic stimulation for Parkinson's disease. *Brain*, *131*(10), 2720–2728. https://doi.org/10.1093/brain/awn214

Weaver, F. M., Follett, K., Stern, M., Hur, K., Harris, C., Marks Jr, W. J., … Group, C. S. P. 468 S. (2009). Bilateral deep brain stimulation vs best medical therapy for patients with advanced Parkinson disease: a randomized controlled trial. *JAMA*, *301*(1), 63–73. https://doi.org/10.1001/jama.2008.929

Wei, L., Hu, X., Yuan, Y., Liu, W., & Chen, H. (2018). Abnormal ventral tegmental area-anterior cingulate cortex connectivity in Parkinson's disease with depression. *Behavioural Brain Research*, *347*, 132–139. https://doi.org/10.1016/J.BBR.2018.03.011

Witt, K., Daniels, C., Reiff, J., Krack, P., Volkmann, J., Pinsker, M. O., … Deuschl, G. (2008). Neuropsychological and psychiatric changes after deep brain stimulation for Parkinson's disease: a randomised, multicentre study. *The Lancet Neurology*, *7*(7), 605–614. https://doi.org/10.1016/S1474-4422(08)70114-5

Witt, K., Daniels, C., & Volkmann, J. (2012). Factors associated with neuropsychiatric side effects after STN-DBS in Parkinson's disease. *Parkinsonism & Related Disorders*, *18*, S168–S170. https://doi.org/10.1016/S1353-8020(11)70052-9

Witt, K., Granert, O., Daniels, C., Volkmann, J., Falk, D., Van Eimeren, T., & Deuschl, G. (2013). Relation of lead trajectory and electrode position to neuropsychological outcomes of subthalamic neurostimulation in Parkinson's disease: Results from a randomized trial. *Brain*, *136*(7), 2109–2119. https://doi.org/10.1093/brain/awt151

Wohlschläger, A., Karne, H., Jordan, D., Lowe, M. J., Jones, S. E., & Anand, A. (2018). Spectral Dynamics of Resting State fMRI Within the Ventral Tegmental Area and Dorsal

bioRxiv preprint doi: https://doi.org/10.1101/665976; this version posted June 10, 2019. The copyright holder for this preprint (which was not certified by peer review) is the author/funder. All rights reserved. No reuse allowed without permission.

Raphe Nuclei in Medication-Free Major Depressive Disorder in Young Adults . *Frontiers in Psychiatry* . Retrieved from https://www.frontiersin.org/article/10.3389/fpsyt.2018.00163

Supplementary Tables:

I. Berlin

PATIENT	AGE/ GENDER	DISEASE DURATION (yrs.)	TYPE OF IPS	MONTHS BETWEEN ASSESSMENTS	LEDD REDUCTION (%)	DOPAMIN AGONIST REDUCTION (%)	ΔBDI-II (abs.)	ΔBDI-II (%)	ΔUPDRS III (% DBS ON VS. OFF – ON MEDICATION)	ELECTRODE TYPE	CONTACTS USED FOR STN DBS	
											L	R
#1	63/m	15	trem.-dominant	12	70.4	0	10	66.7	14.3	Medtronic Activa PC 3389	10-	2-, 3-
#2	56/m	3	equivalent	12	36.1	100	6	66.7	46.7	Boston Scientific Vercise octopolar	12-	4-
#3	72/f	20	equivalent	12	69.1	85.9	-8	-400	88.9	Medtronic Activa PC 3389	9-	1-
#4	70/m	7	akin.-rigid rigid	12	70.7	100	0	0	70.8	Medtronic Activa PC 3389	9-/10-	1-/2-
#5	73/m	3	equivalent	12	67.8	-25	7	43.8	106.25	Medtronic Activa PC3389	8-	1-
#6	69/m	11	akin.-rigid	12	31.6	-	11	73.3	76.9	Medtronic Activa PC 3389	10-/11+	2-, 3-
#7	58/m	13	equivalent	12	88.4	-	0	0	68.2	Medtronic Activa PC 3389	11-	3-
#8	73/m	9	equivalent	12	39.1	100	3	30	33.3	Medtronic Activa PC 3389	11-	3-
#9	72/f	5	brady.-rigid	12	-26	-185.5	-7	-38.9	0	Medtronic Activa PC 3389	10-	0-
#10	65/m	14	akin.-rigid	12	44.4	46.7	4	66.7	77.1	Medtronic Activa PC 3389	8-/9+	0-/1+
#11	63/f	8	trem.-dominant	12	68.9	100	7	50	6.3	Medtronic Activa PC 3389	9-	1-
#12	63/f	8	equivalent	12	56.4	100	-1	-12.5	107.5	Medtronic Activa PC 3389	8-	0-
#13	58/f	8	trem.-dominant	12	18.4	8.9	14	51.8	20	Medtronic Activa PC 3389	9-, 10-	2-
#14	63/m	15	akin.-rigid	12	85.4	100	-5	-62.5	72.7	Medtronic Activa PC 3389	10-/11-	2-/3-
#15	52/m	5	akin.-rigid	12	100	100	-1	-6.7	-22.2	Boston Scientific Vercise Directed	13-/14-/15-	5-/6-/7-
#16	69/f	4	trem.-dominant	12	100	100	-7	-28	-66.7	Boston Scientific Vercise Directed	11-/14-	5-/6-/7-
#17	64/m	9	akin.-rigid	12	40.5	63.4	2	40	82.6	Medtronic Activa PC 3389	9-	1-
#18	50/m	6	akin.-rigid	12	16.3	0	1	8.3	-30	Medtronic Activa PC 3389	9-	1-
#19	61/f	-	equivalent	12	0	0	-3	-20	100	Medtronic Activa PC 3389	11-	3-
#20	63/m	16	akin.-rigid	12	45.6	40	-7	-100	69.2	Medtronic Activa PC 3389	9-	1-
#21	70/m	6	akin.-rigid	12	62.5	83.3	-6	-66.7	172.7	Medtronic Activa PC 3389	9-	1-
#22	61/m	6	akin.-rigid	12	-	-	-2	-66.7	-	Boston Scientific Vercise Directed	2(17%), 3(17%), 4(33%)	10(17%), 11(66%), 12(17%)
#23	41/f	14	trem.-dominant	12	64.3	-50	8	36.4	77.8	Boston Scientific Vercise Directed	3-	13-
#24	52/m	4	akin.-rigid	12	100	-	-7	-46.7	100	Boston Scientific Vercise Directed	3-/4-	11-/12-
#25	54/m	18	akin.-rigid	12	11.6	100	-6	-66.7	0	Boston Scientific Vercise Directed	4-	12-
#26	73/f	8	trem.-dominant	12	39.9	-	-1	-9.1	35	Boston Scientific Vercise Directed	5-/6-/7-	13- /14- /15-
#27	55/m	19	equivalent	12	61.2	100	10	47.6	-	Boston Scientific Vercise Directed	2- (53%), 3- (38%), 4- (9%)	10-(23%), 11-(54%), 12- (23%)
#28	77/m	7	akin.-rigid	12	13.7	100	-2	-25	-34.8	Boston Scientific Vercise Directed	14- (85%), 9- (15%)	1- (15%), 6- (85%)
#29	52/f	12	akin.-rigid	12	45	100	-19	-172.7	80.6	Boston Scientific Vercise Directed	2- (8%), 3- (6%), 4- (6%), 5- (28%), 6- (26%), 7- (26%)	10-(34%), 11-(33%), 12-(33%)
#30	60/m	14	equivalent	12	77.1	69.2	1	14.3	70	Medtronic Activa 3389	10-	2-
#31	61/m	15	equivalent	12	-100	-	-3	-100	67.6	Boston Scientific Vercise Directed	2- (33%), 3- (33%), 4- (34%)	13-(33%), 14-(33%), 15-(33%)
#32	32/m	15	akin.-rigid	12	29.7	36.8	1	20	64.3	Boston Scientific Vercise Directed	6-	11-/12-/13-

IPS – IDIOPATHIC PARKINSON'S SYNDROME; LEDD – LEVODOPA EQUIVALENT DAILY DOSIS; BDI-II – BECK'S DEPRESSION INVENTORY; UPDRS – UNIFIED PARKINSON'S DISEASE RATING SCALE; TREM.-DOMINANT – TREMORDOMINANT; AKIN.-RIGID – AKINETIC-RIGID

II. Queensland

CONNECTIVITY LINKS STN-DBS WITH DEPRESSION

PATIENT	AGE/ GENDER	DISEASE DURATION (yrs.)	TYPE OF IPS	MONTHS BETWEEN ASSESSMENTS	LEDD REDUCTION (%)	DOPAMIN AGONIST REDUCTION (%)	ΔBDI-II (abs.)	ΔBDI-II (%)	ΔUPDRS III (% DBS ON VS. OFF – ON MEDICATION)	ELECTRODE TYPE	CONTACTS USED FOR STN DBS	
											L	R
#1	71/m	6	akin.-rigid	6	65.2	0	0	0	28.3	Medtronic Activa PC 3389	1-	9-
#2	49/m	6	trem.-dominant	6	61.5	0	1	14.3	9.1	Medtronic Activa PC 3390	1+/2-	9+/10-
#3	69/f	4	akin.-rigid	6	66.2	0	8	80	-81.9	Medtronic Activa PC 3391	1-	9-
#4	76/f	15	akin.-rigid	6	59.7	50	7	36.8	28	Medtronic Activa PC 3393	0-	9-
#5	58/m	6	trem.-dominant	6	80.6	0	4	40	-155	Medtronic Activa PC 3394	1-	10-
#6	62/m	12	akin.-rigid	6	67.3	0	8	38	0	Medtronic Activa PC 3395	1-	9-
#7	47/m	7	akin.-rigid	6	71.9	0	3	33.3	-30	Medtronic Activa PC 3396	1-	9-
#8	66/m	6	trem.-dominant	6	78.4	33,33	-15	-125	72.3	Medtronic Activa PC 3397	2-	9-
#9	63/m	3	trem.-dominant	6	100	100	4	100	-12.5	Medtronic Activa PC 3398	1-	9-
#10	56/m	7	akin.-rigid	6	80.5	0	7	43.8	-97	Medtronic Activa PC 3399	1-	9-
#11	67/m	16	trem.-dominant	6	77.8	0	0	0	0	Medtronic Activa PC 3400	2-/3-	10-
#12	35/m	5	trem.-dominant	6	48.6	100	1	12.5	55.3	Boston Scientific Vercise octopolar	2-/5-	10+/11-/12+
#13	68/m	8	akin.-rigid	6	68.1	33,33	-2	-18.2	24.2	Medtronic Activa PC 3389	1-	9-
#14	66/m	16	trem.-dominant	6	59	0	-3	-27.3	-320	Medtronic Activa PC 3389	2-/3-	10-
#15	66/f	9	trem.-dominant	6	70.9	0	8	57.1	-14.3	Medtronic Activa PC 3389	1-/2-	9-
#16	65/m	10	akin.-rigid	6	71	0	-2	-33.3	-17.6	Medtronic Activa PC 3389	0-	10+/9-
#17	69/m	5	akin.-rigid	6	54.1	0	5	50	-26.9	Medtronic Activa PC 3389	1-	9-
#18	65/m	14	trem.-dominant	6	81.4	0	2	50	-21.4	Boston Scientific Vercise octopolar	3-	10+/11-
#19	69/m	12	akin.-rigid	6	49.9	0	12	92.3	-68.8	Boston Scientific Vercise octopolar	2-	10-
#20	72/f	20	trem.-dominant	6	55	0	-4	-44.4	-30.8	Boston Scientific Vercise octopolar	3-/5-	11-
#21	55/f	5	trem.-dominant	6	100	100	-1	-12.5	-69.2	Boston Scientific Vercise octopolar	3-	9-
#22	70/m	5	trem.-dominant	6	63.6	0	4	28.6	29.5	Boston Scientific Vercise octopolar	4-/5-	10+/11-
#23	57/f	2	trem.-dominant	6	100	0	-7	-100	-7.1	Boston Scientific Vercise octopolar	4-	12-
#24	64/m	8	trem.-dominant	6	74.4	-150	8	61.5	26.1	Boston Scientific Vercise octopolar	0+/1-	10-
#25	53/m	5	akin.-rigid	6	72.9	-193,33	12	75	-105.3	Medtronic Activa PC 3389	1+/2-	10+/11-
#26	65/m	6	trem.-dominant	6	0	0	1	6.7	7.4	Boston Scientific Vercise octopolar	3-	10+/11-/13-
#27	60/f	5	trem.-dominant	6	73.9	100	2	14.3	37.5	Boston Scientific Vercise octopolar	5-	12-
#28	61/m	21	akin.-rigid	6	55.8	-50	8	57.1	34.3	Medtronic Activa PC 3389	0-	9-
#29	42/m	3	akin.-rigid	6	85.7	0	7	77.8	-16.7	Boston Scientific Vercise octopolar	2-	10+/11-
#30	60/f	5	akin.-rigid	6	76.2	61,54	-4	-80	34.6	Boston Scientific Vercise octopolar	2-	11+/12-
#31	70/f	6	trem.-dominant	6	76.8	0	-3	-100	7.4	Boston Scientific Vercise octopolar	2-/3-	11-
#32	58/m	8	trem.-dominant	6	47.6	16,67	-9	-75	-34.3	Medtronic Activa PC 3389	2-	10-
#33	71/m	10	trem.-dominant	6	85.8	0	6	35.3	-30.2	Medtronic Activa PC 3389	1-	9-
#34	73/m	5	akin.-rigid	6	73.3	0	7	36.8	14.7	Boston Scientific Vercise octopolar	2-	10+/9-
#35	61/f	9	trem.-dominant	6	70.4	0	2	50	-3.7	Boston Scientific Vercise octopolar	4-	10-
#36	54/f	7	akin.-rigid	6	91	0	10	100	-70.8	Boston Scientific Vercise octopolar	3-	11-
#37	70/f	4	akin.-rigid	6	92	90	4	40	-19.6	Medtronic Activa PC 3389	1-	9-
#38	54/m	9	trem.-dominant	6	85.7	0	10	58.8	24.3	Medtronic Activa PC 3389	1-	9-
#39	54/m	8	akin.-rigid	6	79.5	0	5	41.7	42.9	Boston Scientific Vercise octopolar	2-	10-/11-
#40	69/f	6	akin.-rigid	6	-15	0	2	22.2	23.5	St Jude Directional	3-	11-, 12-

#41	71/m	8	akin.-rigid	6	78.6	25	-3	-75	25.7	St Jude Directional	2-	11-
#42	51/m	17	akin.-rigid	6	89.5	0	8	57.1	-10.5	St Jude Directional	2-	10-
#43	73/m	10	trem.-dominant	6	53.3	25	-2	-18.2	-129.6	St Jude Directional	3-	11-
#44	52/m	9	trem.-dominant	6	63.4	0	2	33.3	-125	St Jude Directional	1-	10-
#45	51/f	7	trem.-dominant	6	18.3	0	3	14.3	14.8	St Jude Directional	3-	11-
#46	77/m	7	trem.-dominant	6	100	0	0	0	-61	St Jude Directional	2-	10-
#47	76/f	11	akin.-rigid	6	96.2	0	5	71.4	-45.8	Boston Scientific Vercise octopolar	3-/4-	12-
#48	70/m	8	mixed	6	54.6	-20	4	57.1	28	Boston Scientific Vercise octopolar	2-	9+/10-

IPS – IDIOPATHIC PARKINSON'S SYNDROME; LEDD – LEVODOPA EQUIVALENT DAILY DOSIS; BDI-II – BECK'S DEPRESSION INVENTORY; UPDRS – UNIFIED PARKINSON'S DISEASE RATING SCALE; TREM.-DOMINANT – TREMORDOMINANT; AKIN.-RIGID – AKINETIC-RIGID;

III. Cologne

PATIENT	AGE/ GENDER	DISEASE DURATION (yrs.)	TYPE OF IPS	MONTHS BETWEEN ASSESSMENTS	LEDD REDUCTION (%)	DOPAMIN AGONIST REDUCTION (%)	ΔBDI-II (abs.)	ΔBDI-II (%)	ΔUPDRS III (% DBS ON VS. OFF – ON MEDICATION)	ELECTRODE TYPE	CONTACTS USED FOR STN DBS	
											L	R
#1	53/f	11	equivalent	11	44	54,72	3	100	-	Medtronic Activa 3389	P1: 0-; P2: 1-	P1: 8-; P2: 9-
#2	50/m	10	akin.-rigid	6	27.5	0	7	100	38.5	Boston Scientific Vercise Directed	5-	13-
#3	61/f	6	akin.-rigid	12	83.3	50	3	30	80	Boston Scientific Vercise Directed	2- (34%), 3- (33%), 4- (33%)	10- (33%), 11- (34%), 12- (33%)
#4	51/f	15	akin.-rigid	5	88.5	66,67	3	50	-100	Boston Scientific Vercise Directed	5- (33%), 6- (33%), 7- (34%)	10- (50%), 11- (50%)
#5	63/f	4	akin.-rigid	6	55	25	-1	-8.3	36.4	Boston Scientific Vercise Directed	5- (33%), 6-(33%), 7- (34%)	10- (33%), 11-(33%), 12-(34%)
#6	54/m	8	akin.-rigid	2	36.9	-33,33	-2	-50	-	Boston Scientific Vercise Directed	1-	15-
#7	71/m	14	akin.-rigid	6	18.8	0	0	0	-155.6	Boston Scientific Vercise Directed	2- (14%), 3-(13%), 4- (13%), 5- (20%), 6- (20%), 7- (20%)	10- (14%), 11- (13%), 12-(13%), 13-(20%), 14-(20%), 15-(20%)
#8	53/f	4	equivalent	5	50.6	0	3	100	-50	Boston Scientific Vercise Directed	8-	16-
#9	61/m	13	equivalent	6	36.8	0	5	45.5	-166.7	Boston Scientific Vercise Directed	1-	9-
#10	64/f	14	akin.-rigid	5	39.8	27,27	-11	-220	63.6	Boston Scientific Vercise Directed	5- (33%), 6- (34%),7- (33%	13- (27%), 14- (45%), 15- (28%)
#11	56/m	4	trem.-dominant	5	43.3	90,19	0	0	-60	Boston Scientific Vercise Directed	5- (40%), 6- (20%), 7- (40%)	13- (26%), 14- (49%), 15- (25%)
#12	68/f	13	akin.-rigid	6	51	0	-1	-16.7	7.4	Boston Scientific Vercise Directed	5- (34%), 6-(33%),7- (33%	10- (30%), 11- (10%), 13- (40%), 14- (20%)
#13	49/f	8	akin.-rigid	5	44	45,81	-9	-450	10	Boston Scientific Vercise Directed	7-	10- (25%), 11- (25%), 12- (5%), 13- (20%), 14- (25%)
#14	57/m	10	trem.-dominant	5	66	37,5	3	50	-34.5	Boston Scientific Vercise Directed	P1: 8-; P2: 4-(20%), 7- (80%)	13-(20%), 14-(40%), 15-(20%), 16-(20%)
#15	72/m	11	akin.-rigid	5	42.2	53,33	-2	-33.3	-58.8	Boston Scientific Vercise Directed	2- (18%), 3- (16%), 4- (16%), 5- (18%), 6- (16%), 7- (16%)	13- (33%), 14- (33%), 15- (34%)
#16	71/f	13	akin.-rigid	6	61	75	0	0	-76.5	Boston Scientific Vercise Directed	13- (27%), 14- (27%), 15- (46%)	2- (25%), 3- (15%), 4- (40%), 5- (10%), 7- (10%)
#17	62/f	12	equivalent	5	47.5	42,86	1	9.1	21	Boston Scientific Vercise Directed	5- (34%), 6-(33%), 7- (33%)	13- (10%), 14-(65%), 15- (25%)

#18	67/m	9	akin.-rigid	5	57.1	50	0	0	55.6	Boston Scientific Vercise Directed	2- (34%), 3- (33%), 4- (33%)	10- (34%), 11- (33%), 12- (33%)
#19	70/m	10	akin.-rigid	5	65.3	75	6	75	57.1	Boston Scientific Vercise Directed	2- (34%), 3- (33%), 4- (33%)	13- (34%), 14- (33%), 15- (33%)
#20	76/f	18	equivalent	6	38.7	-33,76	-13	-325	41.2	Boston Scientific Vercise Directed	2- (34%), 3- (33%), 4- (33%)	10- (34%), 11-(33%), 12- (33%)
#21	59/m	8	akin.-rigid	5	56.3	25	-1	0	-314.3	Boston Scientific Vercise Directed	5- (34%), 6-(33%), 7- (33%)	13- (34%), 14- (33%), 15- (33%)
#22	62/m	9	akin.-rigid	6	59.2	13,33	1	9.1	-52.9	Boston Scientific Vercise Directed	5- (34%), 6-(33%), 7- (33%)	13- (34%), 14- (33%), 15- (33%)
#23	52/m	6	equivalent	6	8.6	0	1	50	-88.9	Boston Scientific Vercise Directed	2- (34%), 3- (33%), 4- (33%)	13- (34%), 14- (33%), 15- (33%)
#24	74/m	21	akin.-rigid	5	48	100	4	40	-13	Boston Scientific Vercise Directed	2- (34%), 3- (33%), 4- (33%)	10- (34%), 11-(33%), 12- (33%)
#25	73/m	11	akin.-rigid	6	61.1	83,33	-4	-28.6	45.5	Boston Scientific Vercise Directed	5- (34%), 6-(33%), 7- (33%)	13- (34%), 14- (33%), 15- (33%)
#26	NaN/m	17	akin.-rigid	6	66	-24,76	1	8,3	-300	Boston Scientific Vercise Directed	2-(10%), 3-(10%), 4-(10%), 5-(24%), 6-(23%), 7-(23%)	10-(10%), 11-(10%), 12-(10%), 13-(24%), 14-(23%),15-(23%)
#27	75/f	10	akin.-rigid	6	26.5	0	-3	-60	31.3	Boston Scientific Vercise Directed	2- (34%), 3- (33%), 4- (33%)	10-(34%), 11-(33%), 12-(33%)
#28	71/f	7	equivalent	6	73.4	66,67	2	33.3	0	Boston Scientific Vercise Directed	2- (10%), 3- (10%), 4- (10%), 5- (24%), 6- (23%), 7- (23%)	10- (10%), 11-(10%), 12- (10%), 13- (24%), 14- (23%), 15- (23%)
#29	63/f	8	equivalent	6	49.4	50	4	25	-17.6	Boston Scientific Vercise Directed	1-	10- (34%), 11-(33%), 12- (33%)
#30	58/f	8	equivalent	5	72.7	0	3	42.9	8	Boston Scientific Vercise octopolar	5-	R: 9-(19%), 10- (39%), 11- (45%)
#31	47/f	8	akin.-rigid	5	22	75	0	0	80	Boston Scientific Vercise octopolar	3-/4-	11- (40%), 12- (30%), 13- (30%)
#32	63/f	13	equivalent	6	63.4	42,86	3	37.5	-54.5	Boston Scientific Vercise octopolar	3-/4-	P1: 11- (25%), 13- (75%); P2: 13-(50%), 14-(50%)
#33	61/m	8	trem.-dominant	5	39.2	0	2	15.4	54.3	Boston Scientific Vercise Directed	5-/6-/7+	13- (50%), 14- (50%), 15+ (100%)
#34	69/f	13	akin.-rigid	5	3.9	43,93	-1	-50	19.2	Boston Scientific Vercise Directed	1-	9-
#35	54/m	9	equivalent	5	41.2	33,33	-5	-38.5	-6,7	Boston Scientific Vercise Directed	2-(10%), 3-(10%), 4-(10%), 5-(24%), 6-(23%), 7-(23%)	10-(10%), 11-(10%), 12-(10%), 13-(24%), 14-(23%), 15-(23%)
#36	61/m	13	akin.-rigid	5	50	100	-14	-200	17.4	Boston Scientific Vercise octopolar	3- (40%), 4- (45%), 5- (15%)	11- (20%), 10- (20%), 12- (20%), 13- (20%), 14- (20%)

IPS – IDIOPATHIC PARKINSON'S SYNDROME; LEDD – LEVODOPA EQUIVALENT DAILY DOSIS; BDI-II – BECK'S DEPRESSION INVENTORY; UPDRS – UNIFIED PARKINSON'S DISEASE RATING SCALE; TREM.-DOMINANT – TREMORDOMINANT; AKIN.-RIGID – AKINETIC-RIGID;

bioRxiv preprint doi: https://doi.org/10.1101/665976; this version posted June 10, 2019. The copyright holder for this preprint (which was not certified by peer review) is the author/funder. All rights reserved. No reuse allowed without permission.

Supplement 1: Heterogeneous distribution an mean absolute BDI change before and under STN-DBS for the three cohorts.